










# Insights into polyamine metabolism: homospermidine is double-oxidized in two discrete steps by a single copper-containing amine oxidase in pyrrolizidine alkaloid biosynthesis

Mahmoud M. Zakaria <sup>1,2,#</sup> Thomas Stegemann <sup>1,#</sup> Christian Sievert <sup>1,†</sup>  
Lars H. Kruse <sup>1,§</sup> Elisabeth Kaltenecker <sup>1</sup> Ulrich Girreser <sup>3</sup> Serhat S. Çiçek <sup>4</sup>  
Manfred Nitz <sup>5</sup> and Dietrich Ober <sup>1,\*†</sup>

- 1 Botanical Institute and Botanic Gardens, Kiel University, Kiel, Germany
- 2 Department of Pharmacognosy, Faculty of Pharmacy, Zagazig University, Zagazig 44519, Egypt
- 3 Department of Pharmaceutical and Medicinal Chemistry, Kiel University, Kiel, Germany
- 4 Department of Pharmaceutical Biology, Kiel University, Kiel, Germany
- 5 Cellular Proteome Research, Helmholtz Centre for Infection Research, Braunschweig, Germany

\*Author for correspondence: [dober@bot.uni-kiel.de](mailto:dober@bot.uni-kiel.de)

†Present address: Eleva GmbH, Freiburg, Germany.

§Present address: Michael Smith Laboratories, University of British Columbia, Vancouver, V6T 1Z4, BC Canada.

#Shared first authorship.

†Senior author

M.M.Z., T.S., and D.O. designed the research. M.M.Z. and C.S. carried out gene cloning. M.M.Z. carried out *in planta* expression, enzyme assays, kinetics, and site-directed mutagenesis. M.M.Z. and T.S. performed *in vivo* isotopic labeling and GC–MS measurements. T.S. performed VIGS and GC–EI–HRAMS measurements. T.S. and C.S. performed RT–qPCR, and L.H.K. and E.K. conducted the bioinformatics analyses. T.S., U.G., S.S.C., and M.M.Z. performed the NMR experiments and M.N. carried out the microsequencing of peptides. M.M.Z., T.S., E.K., and D.O. wrote the manuscript.

The author responsible for distribution of materials integral to the findings presented in this article in accordance with the policy described in the Instructions for Authors (<https://academic.oup.com/plcell>) is: Dietrich Ober ([dober@bot.uni-kiel.de](mailto:dober@bot.uni-kiel.de)).

## Abstract

Polyamines are important metabolites in plant development and abiotic and biotic stress responses. Copper-containing amine oxidases (CuAOs) are involved in the regulation of polyamine levels in the cell. CuAOs oxidize primary amines to their respective aldehydes and hydrogen peroxide. In plants, aldehydes are intermediates in various biosynthetic pathways of alkaloids. CuAOs are thought to oxidize polyamines at only one of the primary amino groups, a process frequently resulting in monocyclic structures. These oxidases have been postulated to be involved in pyrrolizidine alkaloid (PA) biosynthesis. Here, we describe the identification and characterization of homospermidine oxidase (HSO), a CuAO of *Heliotropium indicum* (Indian heliotrope), involved in PA biosynthesis. Virus-induced gene silencing of HSO in *H. indicum* leads to significantly reduced PA levels. By *in vitro* enzyme assays after transient *in planta* expression, we show that this enzyme prefers Hspd over other amines. Nuclear magnetic resonance spectroscopy and mass spectrometry analyses of the reaction products demonstrate that HSO oxidizes both primary amino groups of homospermidine (Hspd) to form a bicyclic structure, 1-formylpyrrolizidine. Using tracer feeding, we have further revealed that 1-formylpyrrolizidine is an intermediate

## IN A NUTSHELL

**Background:** Alkaloids are a group of often structurally complex natural products that are produced by various plants as part of their defense against herbivores. The toxic pyrrolizidine alkaloids (PAs), for example, occur in several species of the borage family and are characterized by a bicyclic structure. Polyamines, simple nitrogen-containing molecules, are involved in alkaloid formation. They are substrate for a class of enzymes, the copper-containing amine oxidases (CuAOs), which convert polyamines to their respective aldehydes and release hydrogen peroxide. We know little about the enzymes involved in PA formation, especially, how the bicyclic ring system is formed. The ring formation requires two independent oxidations and cyclization, suggesting that several enzymes, including CuAOs, might be involved in this step.

**Question:** Are one or more CuAOs involved in the formation of the bicyclic ring system of PAs? Do the resulting aldehydes cyclize spontaneously or is the cyclization an enzyme-controlled process? For our studies we used Indian heliotrope (*Heliotropium indicum*, borage family) as model that produces PAs in the leaves.

**Findings:** We identified a CuAO, now named homospermidine oxidase, that is involved in PA biosynthesis, as its downregulation resulted in reduced alkaloid levels in the plant. Biochemical characterization of this enzyme revealed that it catalyzes not only both oxidations of the substrate polyamine, that is, homospermidine, but also controls the cyclization. The product is the bicyclus, the pyrrolizidine, in its aldehyde form. This can easily be further oxidized, if the hydrogen peroxide produced by the CuAO is not removed during the enzyme reaction.

**Next steps:** Studies should explore the molecular mechanism by which a single enzyme oxidizes homospermidine twice and controls the cyclization of the resulting aldehydes in two discrete steps. Identifying the pathway intermediate will pave the way for deciphering the subsequent reaction steps and understanding the evolution of this plant defense.

in the biosynthesis of PAs. Our study therefore establishes that HSO, a canonical CuAO, catalyzes the second step of PA biosynthesis and provides evidence for an undescribed and unusual mechanism involving two discrete steps of oxidation that might also be involved in the biosynthesis of complex structures in other alkaloidal pathways.

## Introduction

Diamines and polyamines are aliphatic molecules possessing two or more amino groups. Putrescine (Put), spermidine (Spd), and spermine (Spm) are the most common di- and polyamines in seed plants (Chen et al., 2018), whereas others, such as homospermidine (Hspd), are detectable only in small amounts in most angiosperms (Ober et al., 2003). Polyamines are involved in central processes, such as cell growth and proliferation, the regulation of gene expression and translation, membrane stabilization, and apoptosis (Seiler and Raul, 2005; Michael, 2016). Moreover, in plants, polyamines are involved in cell signaling and in response to abiotic and biotic stresses (Chen et al., 2018; Sobieszczuk-Nowicka et al., 2019).

All of these processes require the stringent control of polyamine levels, which are regulated by enzymes including copper-containing amine oxidases (CuAOs, EC 1.4.3.22, formerly called “diamine oxidases”). CuAOs are a group of ubiquitous enzymes that catalyze the oxidative deamination of primary amino groups into their corresponding aldehydes with the concomitant formation of hydrogen peroxide and ammonia (Figure 1A) (Lunelli et al., 2005). The hydrogen peroxide produced is responsible for a plethora of secondary

effects. In plants, these effects include cell-wall reinforcement, lignification during maturation, and stress response reactions, because hydrogen peroxide is part of stress-induced signal transduction (Gross et al., 2017).

The activation of CuAOs requires that a specific tyrosine residue is posttranslationally modified to topaquinone (TPQ) by a self-catalytic process involving enzyme-bound Cu(II) (Johnson et al., 2007). Thus, CuAOs are sensitive to inhibition by carbonyl-group reagents such as hydroxyethylhydrazine or other substituted hydrazines that interact with the TPQ cofactor (Nagakubo et al., 2019).

CuAOs are described as accepting structurally diverse substrates ranging from histamine in animals to cadaverine (Cad) and further polyamines in plants. In several cases, the aminoaldehydes resulting from the CuAO-mediated oxidation of polyamines cyclize spontaneously to form products that have been shown to be important intermediates in various plant pathways (Wanner and Koomen, 1999; Aniszewski, 2007). For example, CuAO-mediated deamination of Put yields 4-aminobutanal that can be further metabolized to  $\gamma$ -aminobutyric acid (GABA) (Figure 1B). Further examples include the oxidative deamination of *N*-methylputrescine to 4-methylaminobutanal, which spontaneously cyclizes to the *N*-

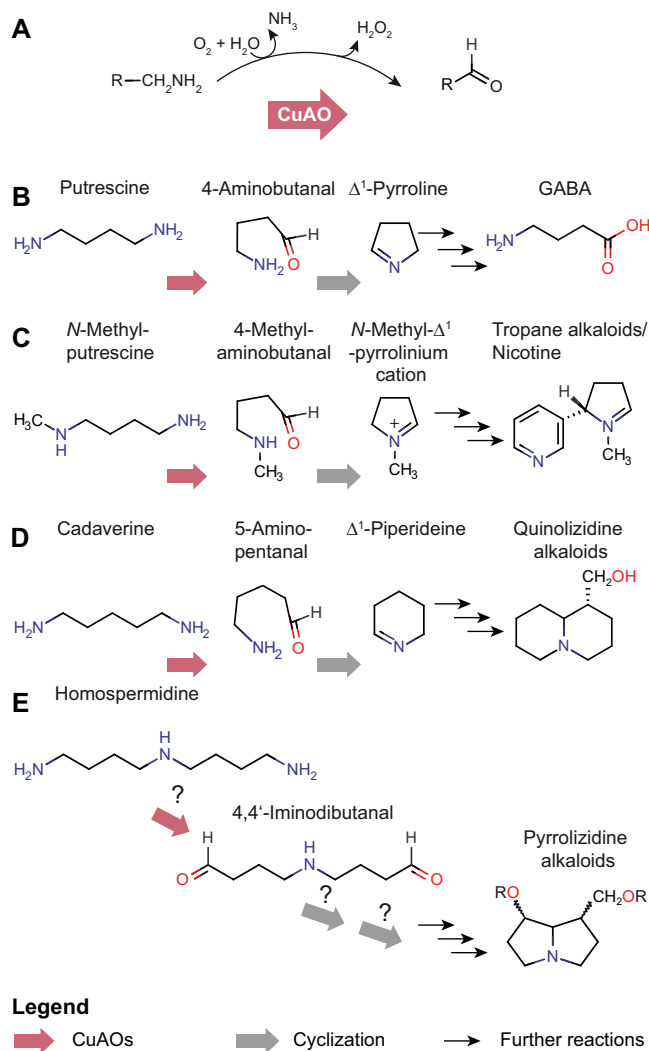


**Figure 1** Oxidation of di- and polyamines by CuAOs and subsequent cyclization of the resulting aldehydes. A, Reaction of primary amines with CuAOs. Their oxidative deamination releases the corresponding aldehyde with parallel production of ammonia and hydrogen peroxide. B, Formation of GABA, a plant signaling molecule, from oxidation of Put. C, Biosynthesis of tropane alkaloids and nicotine requires the oxidation of N-methylputrescine. D, Oxidation of Cad is the first step in the biosynthesis of quinolizidine alkaloids. E, Proposed oxidation of Hspd by CuAOs to 4,4'-iminodibutanal, an intermediate postulated to cyclize to the characteristic bicyclic pyrrolizidine structure of the necine base moiety in PA biosynthesis.

methylpyrrolium cation, an important intermediate in the biosynthesis of nicotine (Heim et al., 2007; Katoh et al., 2007) and tropane alkaloids (Hashimoto et al., 1990) (Figure 1C). Similarly, aminopentanal resulting from the oxidation of Cad is incorporated after cyclization into the biosynthetic route to give quinolizidine alkaloids (Yang et al., 2017) (Figure 1D), lycopodium alkaloids (Ma and Gang, 2004), and piperidine alkaloids (Gerdes and Leistner, 1979). In all these cases, monocyclic structures are formed after the oxidation of a single primary amino group.

CuAOs are also thought to be involved in the biosynthesis of pyrrolizidine alkaloids (PAs). PAs are secondary metabolites that are, like many other alkaloids, part of the chemical defense of plants against herbivores and are produced in various unrelated lineages of angiosperms (Reimann et al., 2004; Kaltenecker et al., 2013). They are esters having a bicyclic necine base with one or more necic acids (Ober and Hartmann, 2000). In the first specific step of PA biosynthesis, an aminobutyl moiety of Spd is transferred to Put to yield Hspd, a reaction catalyzed by Hspd synthase (HSS) (Ober and Hartmann, 1999). In the following steps, CuAOs have been proposed to be involved in the oxidation of Hspd at both primary amino groups resulting in an intermediate postulated to cyclize spontaneously to the characteristic bicyclic pyrrolizidine of the necine base moiety (Böttcher et al., 1993) (Figure 1E). The main arguments in favor of this process are the type of reaction (Khan and Robins, 1985), the inhibition of this step in PA biosynthesis by hydroxyethylhydrazine (Böttcher et al., 1993; Frölich et al., 2007), and a biomimetic experiment in which the incubation of Hspd with a CuAO of pea (*Pisum sativum*) seedlings resulted in detectable amounts of a pyrrolizidine (Robins, 1982).

CuAOs are encoded by small gene families in plant genomes, with 10 annotated genes having been predicted in *Arabidopsis thaliana* (Fraudentali et al., 2019). To identify candidates for an Hspd oxidizing CuAO, co-expression with HSS has been analyzed based on the assumption that the biosynthesis of the PA backbone is restricted to specific cells (Moll et al., 2002; Anke et al., 2004). Of note, HSS shows a highly specific expression pattern in various PA-producing lineages (Moll et al., 2002; Anke et al., 2004, 2008; Niemüller et al., 2012; Kruse et al., 2017). In the model plant studied here, namely *Heliotropium indicum* (Indian heliotrope, Heliotropiaceae), HSS has been localized exclusively in the cells of the lower leaf epidermis and in the epidermis of shoots, whereas no expression has been observed in the upper leaf epidermis (Niemüller et al., 2012). Based on these expression data, the transcriptome of the upper epidermis has been subtracted from that of the lower epidermis resulting in a transcriptome enriched in PA-specific transcripts (Sievert et al., 2015). This transcriptome has been used in this study to screen for candidate CuAOs involved in PA biosynthesis.

Here, we show that one of the CuAOs identified from the subtracted transcriptome is the previously hypothesized Hspd oxidase (HSO) of PA biosynthesis. This enzyme is co-expressed with HSS and its downregulation by virus-induced gene silencing (VIGS) results in significantly reduced PA levels. HSO resulting from expression in *Nicotiana benthamiana* exhibits a substrate preference for Hspd. In-depth *in vitro* analyses with affinity-purified enzyme and tracer feeding experiments have revealed that HSO oxidizes Hspd at both primary amino groups leading to the formation of the pyrrolizidine backbone of PAs.

## Results

### A putative HSO is co-expressed with HSS

Five partial transcripts encoding CuAO-like proteins (CuAO1–5) have been identified in a subtracted transcriptome previously described of *H. indicum* (Sievert et al., 2015). To quantify the co-expression of these candidates with the gene encoding HSS, cells of the upper and lower leaf epidermis were isolated by laser-capture microdissection microscopy for reverse transcription quantitative polymerase chain reaction (RT-qPCR) analyses.

The transcript levels for the gene encoding CuAO1 were approximately 16-fold higher in the lower leaf epidermis than in the upper leaf epidermis, a pattern similar to that observed for the transcript levels of the gene encoding HSS (98-fold difference), suggesting CuAO1 as a potential

candidate for HSO (Figure 2A). Transcript levels of the genes encoding CuAO2–CuAO5 only differed in the lower and upper epidermis by a factor no higher than 2. One of these genes, *cuao2*, was selected for inclusion into further characterization as a control and for comparative reasons.

The partial transcripts of *hso* and *cuao2* from the transcriptome were validated and completed by 5'- and 3'-rapid amplification of cDNA ends PCR techniques. The open reading frames were shown to be 1,986 and 2,304 bp long, respectively. According to the SignalP-5.0 server (Almagro Armenteros et al., 2019b) and the TargetP-2.0 server (Almagro Armenteros et al., 2019a), the HSO protein was predicted to possess an N-terminal signal peptide of 21 amino acids in length directing it to the secretory pathway. A signal peptide was not predicted for CuAO2 (Figure 3A).

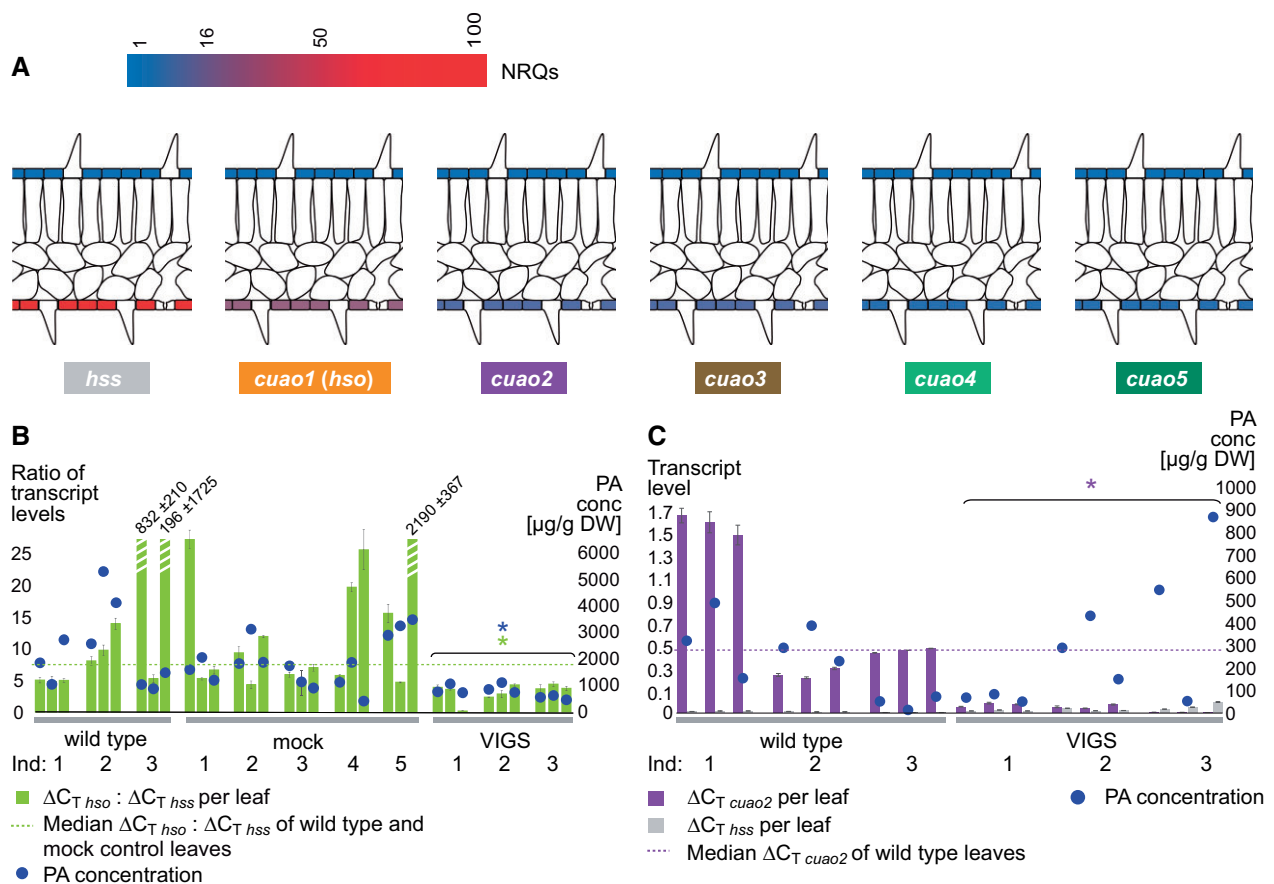


**Figure 2** Relative expression profile of the genes encoding CuAOs in leaves of *H. indicum* wild-type plants and plants subjected to VIGS. **A**, Heat map of the relative expression levels (RT-qPCR; average,  $n = 3$  technical replicates) of the genes encoding CuAOs in upper (control) and lower epidermis of *H. indicum* leaves were compared. *cuao* expression levels were normalized using the geometric mean of three internal reference genes (encoding actin, ubiquitin, elongation factor 1 $\alpha$ ). The *cuao* expression level in the lower epidermis is illustrated by a transformation of the NRQ to the control group (upper epidermis, NRQ control = 1.0) from blue NRQ = 1 to red NRQ = 100. **B**, VIGS of HSO. The transcript levels of the genes encoding HSO and HSS correlate and  $\Delta C_T \text{ hso} / \Delta C_T \text{ hss}$  are shown. Per plant individual, three leaves were separately analyzed. In total, three wild-type, five mock, and three VIGS individuals were analyzed in this experiment. Bar graphs represent the mean  $\pm$  SD of triplicate PCRs from single leaves. The median  $\Delta C_T \text{ hso} / \Delta C_T \text{ hss}$  from wild-type and mock control leaves is given as a horizontal dotted line. The observed high ratios in the wild-type (832 and 196) and mock leaves (2,190) are attributable to extremely low HSS transcript levels (Supplemental Figure S1). The PA content in the analyzed leaves is given by blue dots. Statistically significant differences in transcript and PA levels between wild-type and mock against VIGS individuals are indicated with the color-coded asterisks. **C**, VIGS of CuAO2. Analogous to **B**, except that the transcript levels of the genes encoding CuAO2 ( $\Delta C_T \text{ cuao2}$ ) and HSS ( $\Delta C_T \text{ hss}$ ) are plotted and the median of  $\Delta C_T \text{ cuao2}$  of wild-type leaves is given as a horizontal dashed line. Conc, concentration; DW, dry weight; Ind, individual.

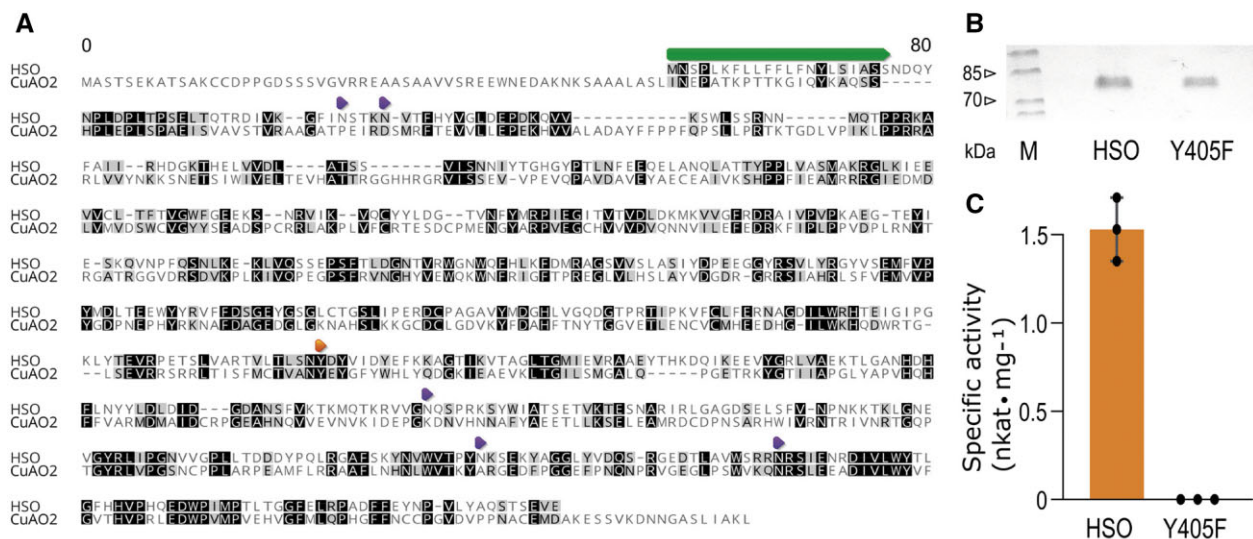


**Figure 3** Structural properties of HSO and CuAO2. **A**, Amino acid alignment of HSO and CuAO2. Identical amino acids and amino acid with a similar residue type (according to the Blosum62 cost matrix) are labeled with black and gray boxes, respectively. The N-terminal signal peptide and the predicted glycosylation sites of HSO are labeled in green and by violet arrowheads, respectively. The tyrosine residue that is modified to TPQ by a posttranslational modification is labeled in orange. The alignment was generated using the Geneious Prime software package (version 2022.0.1, Biomatters Ltd., Auckland, New Zealand). **B**, SDS-PAGE of 0.2  $\mu$ g affinity-purified HSO and the HSO mutant Y405F, in which the tyrosine residue at position 405 was replaced by phenylalanine. Protein bands were stained with Coomassie brilliant blue R-250. M, Unstained Protein Standard, Broad Range (10–200 kDa, New England Biolabs Inc., Ipswich, MA, USA). **C**, Specific activities of HSO and the mutant Y405F. Enzyme activities were determined with the affinity-purified proteins shown in **B** with 1 mM Hspd as substrate. Bar graph represents the mean  $\pm$  SD of activities of three independent transient expression experiments.

### HSO is involved in PA biosynthesis

VIGS was used to test the involvement of HSO in PA biosynthesis. Young leaves of 10-week-old *H. indicum* plants were inoculated with *Agrobacterium tumefaciens* harboring the VIGS-construct for HSO or the empty vector as a negative control (mock). After 14 days, the relative transcript levels of the genes encoding HSO and HSS were estimated in three individual leaves per plant (Figure 2B). *hss* transcript levels varied substantially between wild-type and mock control individuals and even between the leaves of the same individual, indicating the high variability in the activity of PA biosynthesis in *H. indicum* leaves. The same variability was observed for PA levels (Supplemental Figure S1). Of note, despite this high variability, transcript levels of the *hso* gene strongly correlated with that of *hss* ( $P = 0.0003$ , Pearson's product-moment coefficient  $r = 0.678$ ) indicating co-expression as anticipated for genes involved in the same pathway. By relating *hso* to *hss* transcript levels ( $\Delta C_T \text{ hso} / \Delta C_T \text{ hss}$ ), low *hso* transcript levels resulting from the VIGS-mediated effect were discriminated from those that were attributable to the low expression of the whole pathway. Leaves of individuals exhibiting successful knockdown showed significantly lower  $\Delta C_T \text{ hso} / \Delta C_T \text{ hss}$  levels than the leaves of wild-type plants and controls (Figure 2B) (wild-type plus mock versus VIGS plants  $P < 0.0001$  Mann-Whitney test, mock versus VIGS plants  $P < 0.0001$  Mann-Whitney test). These individuals also possessed significantly lower alkaloid levels in the leaves that we analyzed (wild-type plus mock versus VIGS plants  $P = 0.015$ , Welch test, mock versus VIGS plant  $P = 0.0003$  Welch test).

In contrast, in a control experiment (Figure 2C), transcript levels of the gene encoding CuAO2 analyzed in leaves of wild-type plants showed no significant correlation with those of *hss* ( $P = 0.056$ , Pearson's product-moment coefficient  $r = 0.655$ ). In VIGS plants, the transcript levels of the gene *cuao2* were significantly reduced in comparison to wild-type plants (Figure 2C,  $P < 0.0001$ , Mann-Whitney test). This was also observed when *cuao2* transcript levels were normalized to *hss* (Supplemental Figure S1B,  $P < 0.0001$ , Mann-Whitney test). PA levels were not significantly affected by the VIGS-mediated downregulation of the gene encoding CuAO2 ( $P = 0.588$ ). However, PA levels were in general lower compared to the HSO VIGS experiment. An explanation for these differences might be the different seasons at which the two experiments were performed. While the HSO VIGS experiment was performed during summer, CuAO2 VIGS experiment was performed during early spring.

### Transient expression in *N. benthamiana* results in active HSO with a preference for Hspd

Heterologous expression in *Escherichia coli* following strategies described earlier for a CuAO of plant origin, that is the *N*-methylputrescine oxidase from *N. tabacum* (tobacco; Heim et al., 2007; Katoh et al., 2007), failed to provide active HSO protein. Thus, a transient expression system with *N. benthamiana* was established. Quantification of transcript levels in infiltrated *N. benthamiana* leaves by RT-qPCR and of protein levels by gel blot analysis suggested that Days 4 and 6 after infiltration were the optimal time points for

the protein extraction of HSO and CuAO2, respectively (Supplemental Figure S2, A and B). Additionally, a photometric assay for enzyme activity confirmed that the highest activity occurred in desalted crude protein extracts of HSO- and CuAO2-expressing *N. benthamiana* leaves at Days 4 and 6, respectively (Supplemental Figure S2C). These crude extracts were used to screen the substrate preferences of HSO and CuAO2 (Figure 4A). The activity of the HSO-containing crude extract was highest when incubated with Hspd, as was expected for an HSO. However, it also showed activity with the other tested substrates Cad, Put, Spd, and Spm, with activity being weakest with Put (Figure 4A). In contrast, the activity of the CuAO2-containing crude extract was highest when incubated with Put, the favored substrate for many CuAOs thought to be involved in plant primary metabolism (Ghughe et al., 2015; Tavladoraki et al., 2016). This extract showed weak activity with tri- and tetramines. Interestingly, both crude extracts were active with histamine, an amine that contains a monocyclic ring system and that is a known substrate of CuAOs in vertebrates (Hough and Leurs, 2006). The extracts from leaves infected with the empty vector showed no detectable activity with any of the tested substrates (Figure 4A).

Affinity-purified enzyme preparations were used to estimate kinetic properties. As purification resulted in an extremely low yield, we only tested substrates described as being possible metabolites of interest for PA biosynthesis in *H. indicum*, that is, Hspd, Spd, and Put (Frölich et al., 2007). Lineweaver–Burk plot approximation with substrate concentrations up to 9 mM resulted in  $K_M$ -values of 80  $\mu$ M for HSO with Hspd and 4.9 mM for CuAO2 with Put (Figure 4, B and C, Supplemental Table S1). Of note, HSO showed strong inhibition for Put at concentrations higher than

150  $\mu$ M (Supplemental Figure S3). To allow rough comparisons of the kinetic efficiency and substrate preferences of HSO, the ( $k_{cat}/K_M$ ) values denoting the specificity constant were calculated using both linear and nonlinear regression models. In both models, HSO showed the best efficiency with Hspd and substrate preference for Hspd. Additional kinetic parameters for HSO and CuAO2 are summarized in Supplemental Table S1.

### Posttranslational modifications (PTMs) are important prerequisites of active HSO

To gain additional insights into the reaction mechanism of HSO and to determine whether HSO was a canonical CuAO, we further analyzed by liquid chromatography – mass spectrometry (LC-MS) tryptic peptides of HSO purified from HSO-expressing *N. benthamiana* leaves. These analyses confirmed the presence of the predicted N-terminal signal peptide, because only peptides were detected that correspond to the protein starting with amino acid 21 (Figure 3A). Electrospray ionization tandem MS (ESI–MS/MS) of the peptides resulting from trypsin-digested HSO supported that tyrosine 405 ( $^{405}Y$ ) was modified to TPQ. An unmodified and a dihydroxylated octadecapeptide (TVLTLSN $^{405}Y$ DYVIDYEFKK), possibly representing an intermediate of TPQ formation (Rinaldi et al., 1998), were detected (Supplemental Figure S4, A and B). To verify the modification of  $^{405}Y$  to TPQ, HSO was treated with the inhibitor phenylhydrazine, which binds irreversibly to TPQ (Sebela and Sayre, 2009), before digestion with trypsin. An analysis of the resulting peptides detected the same octadecapeptide as before with the expected mass increment of 120 characteristic for the phenylhydrazine adduct of  $^{405}Y$  (Supplemental Figure S4C). Evidence for the need of TPQ

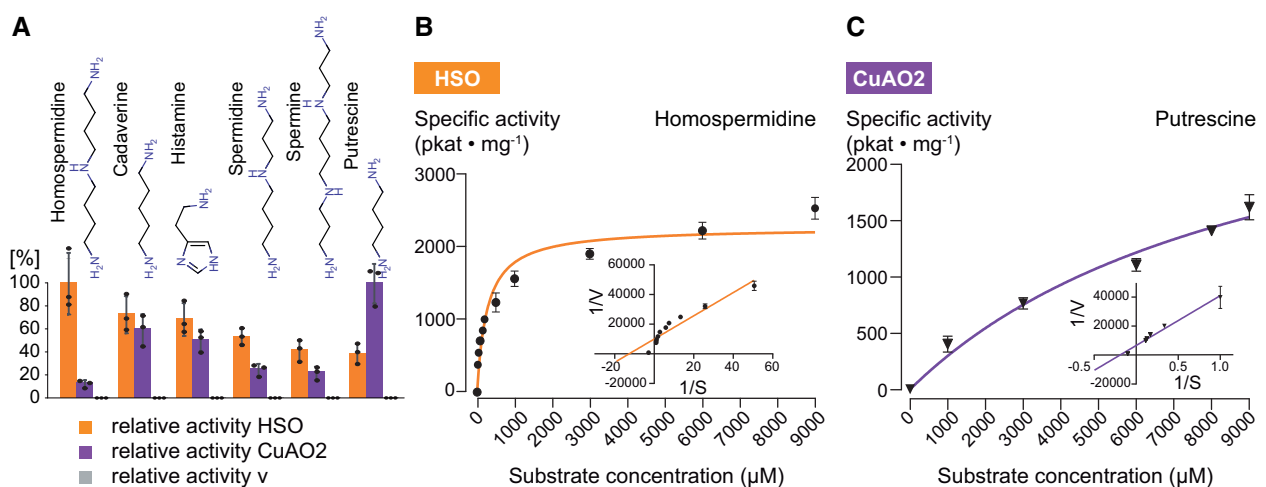


**Figure 4** Biochemical properties of HSO and CuAO2. A, Substrate preference of HSO and CuAO2 toward various diamines and polyamines. Enzyme activity was determined for desalted crude protein extracts of *N. benthamiana* leaves transiently expressing HSO and CuAO2, respectively, by photometric assay with 1 mM substrate in comparison to leaves infected with the empty vector control (v). 100% values correspond to 164.0 pkat/mg for HSO and to 67.4 pkat/mg for CuAO2. Bar graphs represent the mean  $\pm$  SD of activities analyzed with enzyme preparations resulting from three independent transient expression experiments. B and C, Michaelis–Menten plot with an inset Lineweaver–Burk plot for affinity-purified HSO with Hspd as substrate (B) and for affinity-purified CuAO2 with Put as substrate (C). All data points in B and C represent the mean  $\pm$  standard error of the mean (SEM) of values obtained with affinity-purified enzyme prepared from three independent transient expression experiments.

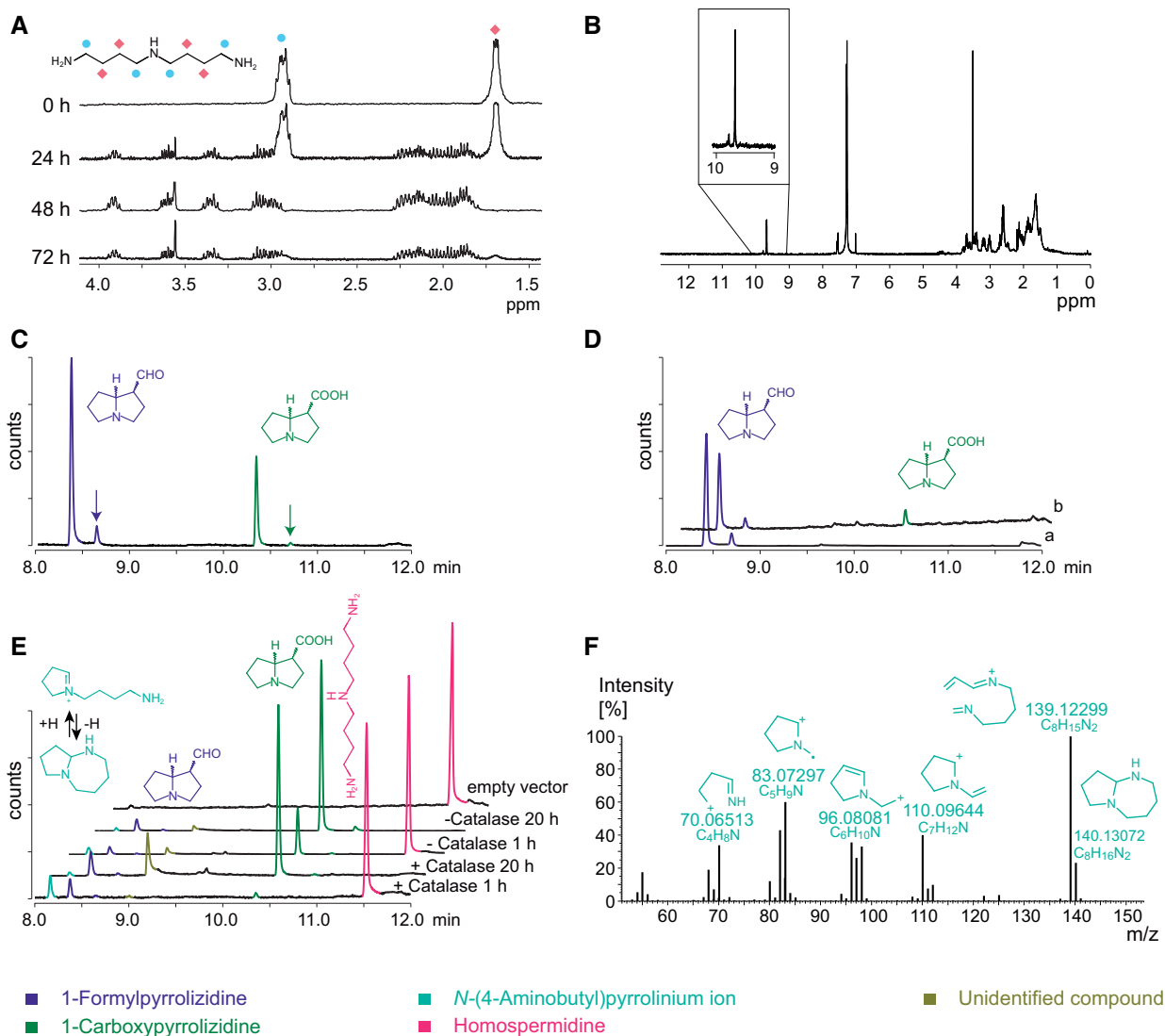


**Figure 5** Identification of reaction products resulting from incubation of HSO with Hspd. For the incubations, affinity-purified HSO (A–D) and desalted crude protein extracts of HSO-expressing *N. benthamiana* leaves (E) have been used. A, Conversion of Hspd by HSO analyzed by 1D proton NMR (in  $\text{D}_2\text{O}$ ) at various time points of the enzyme reaction (0, 24, 48, and 72 h). Spectra are shown for the region of 1.40–4.10 ppm. At the start of the enzyme reaction (0 h), the spectrum shows the hydrogen atoms (1.65–1.70 and 2.90–3.00 ppm) of Hspd. Protons of Hspd in similar chemical environments and the corresponding proton signals in the spectrum are indicated by color-coded circles and diamonds. At the end of incubation (72 h), no hydrogen atoms of Hspd were detectable. Instead, the complex multiplet signals indicate the formation of the pyrrolizidine backbone. The tentative assignment is given in [Supplemental Figure S6C](#). B,  $^1\text{H}$  NMR spectrum of the HSO reaction product mixture (in  $\text{CDCl}_3$ ) displaying typical aldehyde signals at 9.68 and 9.78 ppm in a ratio of about 10:1, respectively, for the two isomers of 1-formylpyrrolizidine. C, GC–MS total ion chromatogram (TIC) of the purified HSO reaction product mixture after 72 h of incubation showing four peaks, namely two early eluting peaks with a specific  $m/z$  of 139, and two later eluting peaks with  $m/z$  of 155, consistent with the two stereoisomers of 1-formyl- and 1-carboxypyrrolizidine, respectively. The arrows point to the minor isomers. D, GC–MS TIC as in C, but the HSO-catalyzed conversion of Hspd occurred in the presence of catalase (a). Only the two isomers of 1-formylpyrrolizidine are detectable, which could be converted to 1-carboxypyrrolizidine by addition of  $\text{H}_2\text{O}_2$  (b). E, GC–MS TICs of various reaction set-ups of HSO with Hspd after 1 and 20 h incubation with and without catalase. In addition to 1-formylpyrrolizidine and 1-carboxypyrrolizidine, an early eluting peak is detectable that represents the deprotonated pyrrolinium ion resulting from cyclization after the oxidation of Hspd at only one of the two primary amino groups. F, Fragmentation pattern of the deprotonated pyrrolinium ion ( $\text{C}_8\text{H}_{16}\text{N}_2$ ) with  $m/z$  of 140 determined by GC–EI–HRAMS.

formation for the enzymatic activity of HSO was provided by the observation that both the replacement of  $^{405}\text{Y}$  by phenylalanine (Figure 3, B and C) and the incubation with 2-hydroxyethylhydrazine resulted in an inactive enzyme.

In addition,  $N$ -glycosylation was detected by ESI–MS/MS for HSO. From five potential  $N$ -glycosylation sites within HSO (asparagine residues at position 48, 52, 492, 576, and 603; Figure 3A),  $\text{Man}_8\text{GlcNAc}_2$  structures were detected at

least at positions 48, 52, and 576, in addition to other high-mannose-type *N*-glycans, as the prominent type of glycosylation (Supplemental Figure S5). The peptide containing the predicted position 492 was only found in an unmodified state, whereas the glycosylation status of position 603 could not be determined unambiguously with the method applied.

### HSO is sufficient for the formation of the methyl-pyrrolizidine backbone

To identify HSO reaction products *in vitro*, 1D proton nuclear magnetic resonance spectroscopy (NMR) was used in a reaction set-up with affinity-purified HSO. The NMR spectra of the HSO reaction showed full turnover after 72 h and indicated the formation of a pyrrolizidine skeleton (Figure 5A). Data from 2D NMR experiments supported this interpretation and suggested the product to be a mixture of 1-formylpyrrolizidine and 1-carboxypyrrolizidine in an approximate ratio of 2:1, respectively (Supplemental Figure S6). An  $^1\text{H}$ ,  $^{13}\text{C}$  heteronuclear single quantum correlation (HSQC) spectrum of the 2D NMR that was performed in an aqueous buffer system indicated the presence of the hydrated aldehyde for the signal at 5.00 ppm ( $^1\text{H}$ ) and 90.9 ppm ( $^{13}\text{C}$ ), respectively (Supplemental Figure S6A). A coupling of this signal at 5.00 ppm with a proton of the broad multiplet at 2.27 ppm was found in the H,H-COSY spectrum, indicating a correlation with the pyrrolizidine backbone (Supplemental Figure S6B). 1D proton NMR and HSQC spectra of the purified reaction product reconstituted in  $\text{CDCl}_3$  displayed typical aldehyde signals at 9.68 ppm ( $^1\text{H}$ ) (Figure 5B) and 202.3 ppm ( $^{13}\text{C}$ ) (Supplemental Figure S7), respectively. Of note, the 1D proton NMR spectrum of the purified product indicated the presence of another minor aldehyde signal at 9.78 ppm related to the pyrrolizidine structure (Figure 5B). As the pyrrolizidine backbone possesses two stereocenters at C1 and C8, respectively, this signal is interpreted as being derived from a second stereoisomer. These two stereoisomers occur in a ratio of approximately 10:1. No signals interpretable as being derived from further stereoisomers were detected.  $^{13}\text{C}$ -NMR confirmed the presence of a quaternary carboxylic acid function at the C9 group of the pyrrolizidine, in addition to the pyrrolizidine with the aldehyde group (Supplemental Figure S8A).

To confirm that the HSO-catalyzed oxidation resulted in the deamination of the two terminal primary amino groups,  $^{15}\text{N}$ - $^1\text{H}$  heteronuclear multiple-bond correlation spectroscopy (HMBC) experiments were performed with fully labeled [ $^{15}\text{N}$ ]Hspd (Supplemental Figure S9). Only a signal of one N atom was detected as a part of the pyrrolizidine after incubation with the HSO (Supplemental Figure S10). This N atom was derived from the secondary amino group of Hspd, whereas the signal derived from the two primary amino

groups disappeared through the HSO-catalyzed double oxidation.

Gas chromatography–MS (GC–MS) analyses of the purified product mixture were conducted to verify the NMR interpretations (Figure 5C). Four peaks could be detected. The two early eluting peaks had a specific mass-to-charge ratio ( $m/z$ ) of 139, whereas the two later eluting peaks had an  $m/z$  of 155, consistent with 1-formyl- and 1-carboxypyrrolizidine, respectively. The two pairs of signals represented the two stereoisomers in an approximate ratio of 10:1, consistent with the NMR data. 1-Formylpyrrolizidine was the major reaction product.

The molecular masses of the reaction products, determined by GC–Electron Impact–High Resolution Accurate MS (GC–EI–HRAMS), were 139.09970 and 155.09463 u, in precise agreement with the calculated masses of 1-formylpyrrolizidine ( $\text{C}_8\text{H}_{13}\text{NO}$ , 139.09971) and 1-carboxypyrrolizidine ( $\text{C}_8\text{H}_{13}\text{NO}_2$ , 155.09463), respectively.

The functional groups of these reaction products were additionally confirmed by derivatization with methoxyamine (MOX) hydrochloride and *N*-methyl-*N*-(trimethylsilyl)trifluoroacetamide (MSTFA), followed by GC–MS analyses. Signals were detected with an  $m/z$  of 168, corresponding to the oxime of 1-formylpyrrolizidine, and an  $m/z$  of 227, corresponding to the trimethyl silylated 1-carboxypyrrolizidine (Supplemental Figure S11). Of note, the stereoisomers were also detected.

### Hydrogen peroxide resulting from the HSO-catalyzed reaction is responsible for *in vitro* oxidation of 1-formylpyrrolizidine

The formation of 1-carboxypyrrolizidine as a reaction product following the *in vitro* incubation with HSO was unexpected as, according to the canonical reaction mechanism of CuAOs, the oxidative deamination of polyamines should result in an aldehyde (Medda et al., 2009; Figure 1). To determine whether the acid was a result of the direct catalytic activity of HSO or attributable to a nonenzymatic reaction of the aldehyde with hydrogen peroxide accumulating as part of the HSO-catalyzed *in vitro* reaction, product identification was set up as described above, except that catalase, as an enzyme eliminating hydrogen peroxide, was added repeatedly to the reaction mixture. Product analysis by  $^{13}\text{C}$ -NMR showed almost identical spectra to those described for incubation without catalase, but lacked the signal for the carboxyl group (Supplemental Figure S8B). Of note, the signal at 91 ppm that was interpreted to result from the hydrated aldehyde group of 1-formylpyrrolizidine was still detectable. The interpretation that 1-formylpyrrolizidine was the sole product resulting from the HSO reaction was confirmed by GC–MS analyses of the purified product (Figure 5D). Additional evidence for artificial conversion was



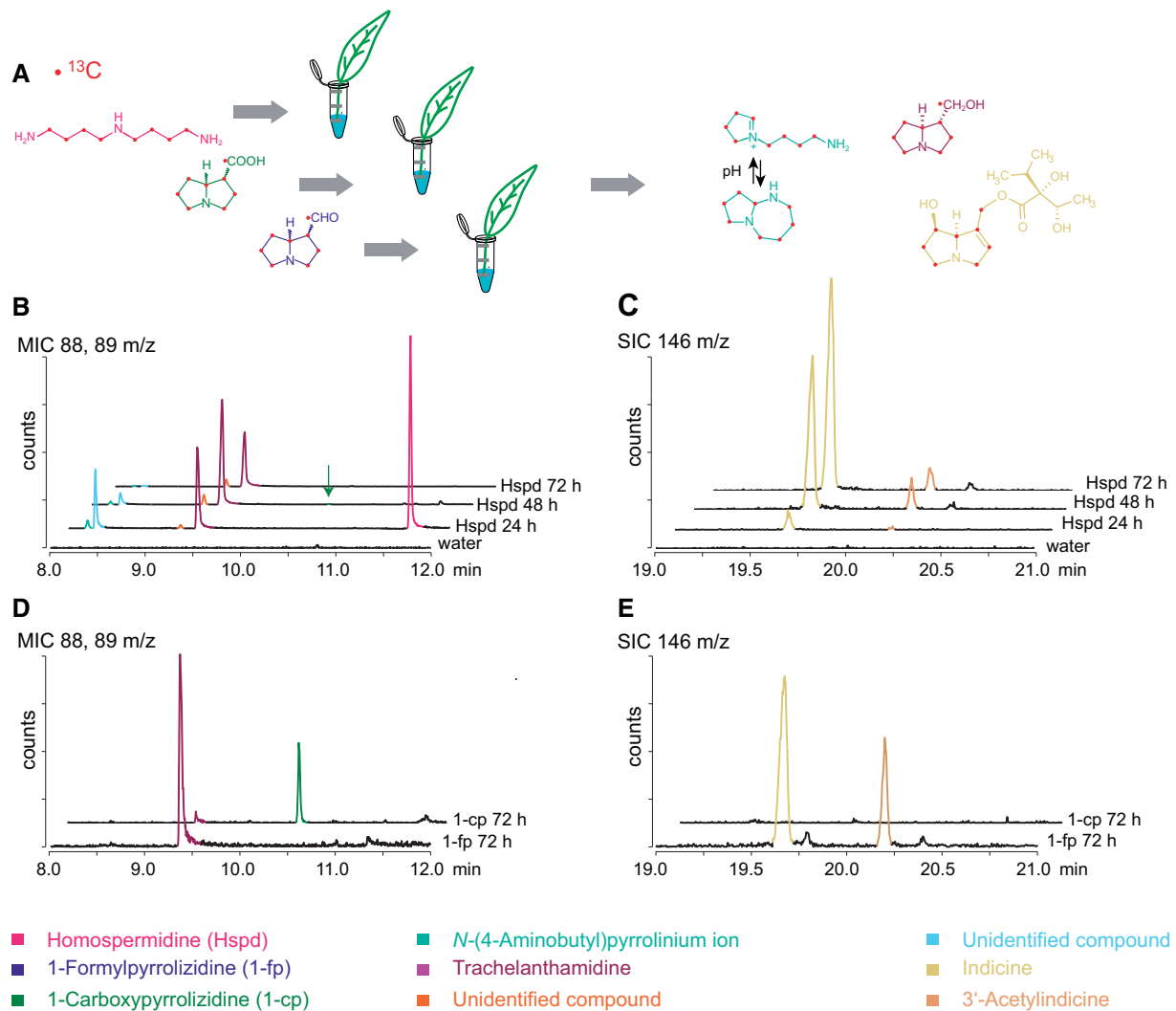


**Figure 6** Tracer feeding experiments. A, Structures of the fully labeled tracers ( $[^{13}\text{C}]$ Hspd,  $[^{13}\text{C}]$ 1-formylpyrrolizidine, and  $[^{13}\text{C}]$ 1-carboxypyrrolizidine) and the detected intermediates and products indicating the labeled carbon atoms (red dots). Multiple ion chromatograms (MICs, B) and single ion chromatograms (SICs, C) of leaf extracts after feeding with  $[^{13}\text{C}]$ Hspd for various time intervals for the masses  $m/z$  of 88, representing the base peak for labeled bicyclic intermediates, and  $m/z$  of 89, representing the base peak of  $[^{13}\text{C}]$ Hspd and  $^{13}\text{C}$ -labeled monocyclic intermediates (B) and for the mass  $m/z$  of 146 characteristic for the  $^{13}\text{C}$ -labeled PA indicine and its derivatives, i.e., the prominent PAs in *H. indicum* (Frölich et al., 2007) (C). The arrow in B points to a small peak of  $[^{13}\text{C}]$ 1-carboxypyrrolizidine. MICs (D) and SICs (E) of leaf extracts after feeding with labeled  $[^{13}\text{C}]$ 1-formylpyrrolizidine (1-fp) and  $[^{13}\text{C}]$ 1-carboxypyrrolizidine (1-cp) for 72 h, analogous to B and C.

provided by the observation that 1-carboxypyrrolizidine was detected when purified 1-formylpyrrolizidine was incubated with hydrogen peroxide (Figure 5D).

### HSO-catalyzed double-oxidation of Hspd involves a monocyclic intermediate

To characterize the HSO-catalyzed reaction further for possible early intermediates of the reaction, GC–MS analyses of reactions with Hspd in the presence and absence of catalase were performed after incubation times of only 1 and 20 h. Desalted crude protein extracts of HSO-expressing *N. benthamiana* leaves and of leaves infected with the empty vector control were used instead of purified protein in order to reduce the manual steps in the experimental set-up. The

previously identified reaction products of 1-formylpyrrolizidine and 1-carboxypyrrolizidine could be detected after only 1 h of incubation, with 1-formylpyrrolizidine being the prominent peak in the incubation with catalase (Figure 5E). After 20 h of incubation, Hspd was completely converted, and 1-carboxypyrrolizidine was the dominating product in both reactions, irrespective of the addition of catalase. Furthermore, an early eluting peak was detectable in all incubations with a  $m/z$  of 140 and a specific fragmentation pattern matching the deprotonated form of the *N*-(4-aminobutyl)pyrrolinium ion (Figure 5F). Its identity was confirmed by GC–EI–HRAMS, which revealed a mass of 140.13077, matching the calculated mass of 140.13080 u for the deprotonated pyrrolinium ion ( $\text{C}_8\text{H}_{16}\text{N}_2$ ). This *N*-(4-aminobutyl)pyrrolinium ion resulted from the cyclization taking

place after the oxidation of Hspd at only one of the two primary amino groups and was detected in its deprotonated form because of the alkaline sample preparation, an observation described earlier (Houen et al., 2005).

### 1-Formylpyrrolizidine is a pathway intermediate and incorporated into PAs

Feeding experiments with [ $^{13}\text{C}$ ]-labeled substrates were performed to study the HSO-catalyzed reaction *in planta*. Putative intermediates and products of PA biosynthesis were analyzed by GC–MS (Figure 6A). Non-natural isotopic shifts in the MS spectra allowed the tracking of the incorporation of the tracer into the various intermediates. After the feeding of [ $^{13}\text{C}$ ]Hspd to fully developed leaves of *H. indicum*, [ $^{13}\text{C}$ ]Hspd was only detectable in the leaves after 24 h (Figure 6B). [ $^{13}\text{C}$ ]Trachelanthamidine was determined in leaves after 24, 48, and 72 h, with the strongest signal after 48 h. [ $^{13}\text{C}$ ]Indicine and its 3'-acetyl derivative, the main PAs in *H. indicum* (Frölich et al., 2007), could be found as early as 24 h after feeding. The size of the peaks of these PAs steadily increased until the maximum incubation time of 72 h (Figure 6C). Traces of 1-carboxypyrrolizidine were observed only after 48 h of incubation (Figure 6B, arrow). 1-Formylpyrrolizidine, the product of *in vitro* incubations of HSO with Hspd, was undetectable. Instead, the *N*-(4-aminobutyl)pyrrolinium ion was detected with the strongest signal being found after 24 h followed by a decrease with longer incubation times (Figure 6B).

The feeding of [ $^{13}\text{C}$ ]-labeled 1-formylpyrrolizidine and 1-carboxypyrrolizidine, respectively, confirmed the incorporation of each of the substrates into trachelanthamidine after 72 h (Figure 6D). Of note, 1-formylpyrrolizidine was incorporated at a higher rate, being completely converted by the end of the experiment, whereas 1-carboxypyrrolizidine, although being taken up into the leaf, remained detectable (Figure 6D). Labeled indicine and its 3'-acetyl derivative were only observed after the feeding of 1-formylpyrrolizidine (Figure 6E).

Taken together, these results suggest that the monocyclic *N*-(4-aminobutyl)pyrrolinium ion and 1-formylpyrrolizidine are the native *in vivo* intermediates in PA biosynthesis.

## Discussion

Polyamines are interconnected with almost all aspects of plant growth, development, and responses to stress (Moschou et al., 2012). CuAOs oxidizing di- and polyamines are key players in polyamine action, not only in primary metabolism but also in several biosynthetic pathways of alkaloids. For example, the biosynthetic routes of tropane alkaloids and quinolizidine alkaloids start from simple diamines like Put and Cad (Lichman, 2021). The early steps in their pathway are the most crucial as they act as a gateway to a new chemical space and direct the metabolic flux away from primary and into specialized metabolism (Lichman, 2021). For PA biosynthesis, the involvement of CuAOs in the oxidation of Hspd was postulated several decades ago (Robins, 1982; Khan and Robins, 1985). Taking these ideas

and findings as our base, we have been able to identify an HSO involved in PA biosynthesis in the PA-producing plant *H. indicum*. The identified enzyme has all characteristics of a typical CuAO. The enzyme oxidizes Hspd at both primary amino groups to form 1-formylpyrrolizidine, a compound readily incorporated into PAs as shown by tracer-feeding experiments.

### HSO has posttranslational modifications characteristic for CuAOs

The heterologous expression of plant CuAOs seems to provide a challenge, as the protocols given in the literature are exceptionally diverse and optimized for each particular enzyme (Koyanagi et al., 2000; Heim et al., 2007; Katoh et al., 2007; Zarei et al., 2015). Our successful *in planta* expression of HSO suggests that the PTMs that are possible in a eukaryotic expression system have a positive effect on the proper folding and activity of the recombinant protein. One such PTM characteristic for CuAOs is the formation of a TPQ that we have been able to detect at tyrosine 405 in the HSO. By replacing this tyrosine with phenylalanine, we have shown that this PTM is essential for the activity of HSO (Figure 3). Furthermore, extensive glycosylations have been described for the CuAOs of various organisms, with estimates that up to 14% of the total molecular weight is attributable to carbohydrates (Tipping and McPherson, 1995; Lunelli et al., 2005). For the HSO of *H. indicum*, we have shown that at least three of the five predicted glycosylation sites are glycosylated with high-mannose-type *N*-glycans, structures also reported for other plant CuAOs (Franc et al., 2013). The observed glycosylation pattern results from heterologous expression in *N. benthamiana* leaves; however, we assume them to be similar to the native glycosylation because of the high conservation of complex *N*-glycan modifications across angiosperms (Strasser, 2016).

### HSO is a CuAO with substrate preference for Hspd

Plant CuAOs are known to accept a wide range of substrates with a preference for diamines having a short chain length of 5–7 carbon atoms (Pietrangeli et al., 2007; Tavladoraki et al., 2016). In this study, we have demonstrated that the preferred substrate of HSO is Hspd, whereas that of CuAO2 is Put, although all other tested substrates are also accepted by HSO (Figure 4A). Such a preference for polyamines that are not part of the polyamine pool of primary metabolism has also been reported for CuAOs involved in other alkaloid biosynthetic pathways (Hashimoto et al., 1990; Yang et al., 2017). Differences in the preference for the various substrates become more obvious from our kinetic analyses. Our data show that HSO is inhibited substantially by Put concentrations higher than 150  $\mu\text{M}$ , whereas with Hspd, no inhibition is detectable for concentrations up to 9 mM. Substrate inhibition has been previously described for various CuAOs and is thought to be attributable to a binding of cationic substrates to the reduced, catalytically incompetent enzyme form that results from the reductive half reaction (Bardsley et al., 1973;

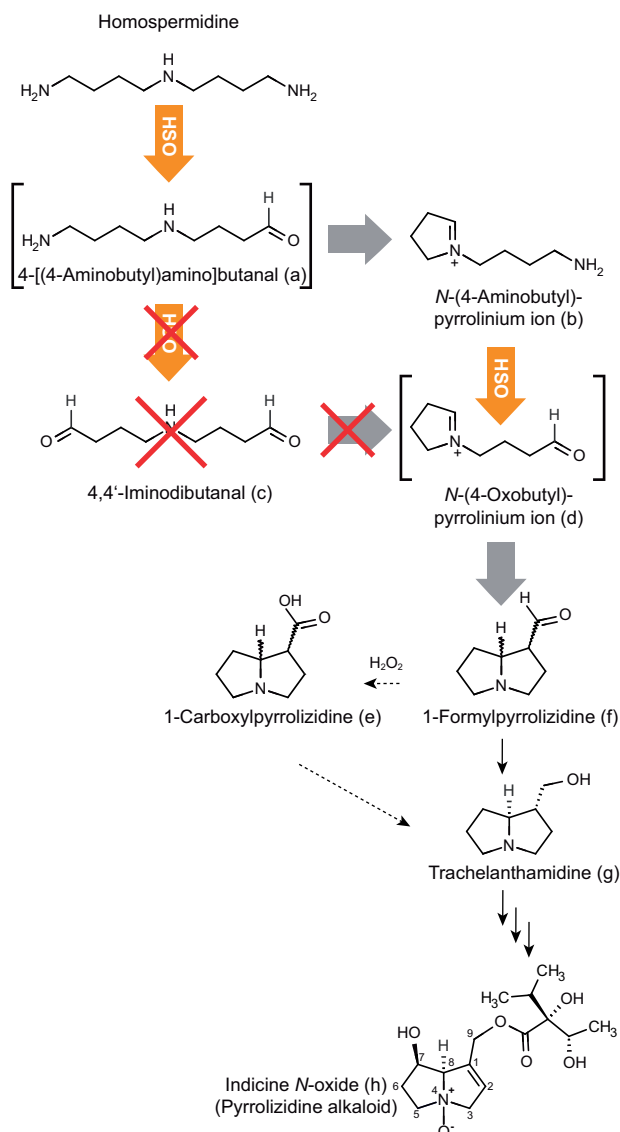


**Figure 7** Proposed pathway for the biosynthesis of the necine base moiety of PAs starting with the HSO-catalyzed oxidation of Hspd according to the current work. HSO catalyzes the oxidation of one of the primary amino groups of Hspd giving the corresponding aldehyde (a), which cyclizes to form the pyrrolinium ion (b), a product previously shown to be the product after incubation with bovine serum amine oxidase (Houen et al., 2005). HSO accepts the pyrrolinium ion again as a substrate and catalyzes a second oxidation, releasing the corresponding aldehyde (d), which cyclizes to form 1-formylpyrrolizidine (f), a structure that is successfully incorporated into indicine N-oxide (h), a characteristic PA found in *H. indicum* leaves. Structures shown in square brackets (a, d) are hypothetical intermediates of this reaction and were not detected in our analyses, but their formation is a prerequisite for proceeding to the detected intermediates. 1-Carboxypyrrolizidine (e) results from the oxidation of 1-formylpyrrolizidine by co-evolving hydrogen peroxide and might also be a direct precursor of indicine N-oxide (h) as it shows slow incorporation into trachelanthamidine (g), but subsequent incorporation into the final PA could not be shown during the feeding period. The discussed alternative biosynthetic routes are shown by dashed arrows. The involvement of the linear dialdehyde (c) as an intermediate of PA biosynthesis was ruled out by the data obtained in this study.

Ignesti, 2003). However, the inhibition observed with Put in concentrations as low as the micromolar range is remarkable, because other CuAOs typically show inhibition only with substrate concentrations in the millimolar range (Ignesti, 2003). Furthermore, based on kinetic analyses of pig kidney CuAO with one- and two-substrate reactions, CuAOs have been postulated to have two substrate-binding sites, only one of which is catalytic (Ignesti, 2003). Whether HSO of *H. indicum* shows such characteristics has not been evaluated in this study. However, as a consequence, the use of the Michaelis–Menten approximation is not recommended for CuAOs (Ignesti, 2003). Nevertheless, the use of various kinetic models to determine variable kinetic parameters with lower substrate concentrations, well before inhibition becomes prominent, has enabled us to confirm the highest specificity and catalytic efficiency of HSO for Hspd over all other tested substrates.

### Biosynthesis of the pyrrolizidine backbone involves two oxidations in two discrete steps

The formation of the bicyclic pyrrolizidine backbone of PAs requires the oxidative deamination of both primary amino groups of Hspd. Therefore, one or two CuAOs might be involved in the oxidation of Hspd. Our data show that a single CuAO, that is HSO, catalyzes the oxidation at both ends of Hspd with the subsequent formation of 1-formylpyrrolizidine as a direct product. Here, we demonstrate that the two oxidative reactions of HSO require the binding of two quite different substrates, namely Hspd and a monocyclic pyrrolinium ion. We are aware of only one other case involving the oxidation of a polyamine at both primary amino groups, that is, the oxidation of Spm, a reaction catalyzed by a CuAO in lentil (*Lens culinaris*) seedlings, with no hints of subsequent cyclizations (Cogoni et al., 1991).

Based on our data, we propose a mechanism with two discrete subsequent oxidations catalyzed by HSO (Figure 7). Our hypothesis is supported by the detection of the monocyclic *N*-(4-aminobutyl)pyrrolinium ion, an intermediate resulting after the oxidation of Hspd at only one of the two primary amino groups, in the *in vitro* assays of HSO and *in planta* after the feeding of [ $^{13}\text{C}$ ]Hspd to fully developed leaves of *H. indicum*. Furthermore, the *in vitro* and *in planta* experiments show that, with longer incubation times, the pyrrolinium ion is consumed to form the bicyclic intermediates of PA biosynthesis. This agrees with earlier studies describing this pyrrolinium ion as being efficiently incorporated into PAs (Kelly and Robins, 1988). Of note, the pyrrolinium ion has also been detected as the end product of the incubation of Hspd with the bovine serum amine oxidase (BSAO) (Houen et al., 2005). In these experiments, the monocyclic *N*-(4-aminobutyl)pyrrolinium ion was not a substrate for BSAO so that the second primary amino group of Hspd was not oxidized. In contrast, HSO accepts the pyrrolinium ion as a substrate and oxidizes the second primary amino group to form the characteristic bicyclic pyrrolizidine backbone. We conclude that HSO should have a substrate

channel that allows the binding of both Hspd and the monocyclic pyrrolinium to the active site to enable the two oxidations. This interpretation is based on structural data published for the CuAOs of pea (*P. sativum*) seedlings and of other eukaryotes that support the interpretation of Ignesti (2003) that CuAOs have only one catalytic site per subunit that is defined by the TPQ and the copper ion (Kumar et al., 1996; Li et al., 1998; Lunelli et al., 2005). Moreover, we have found no evidence for the occurrence of 4,4'-iminodibutanal, an intermediate postulated in the formation of the bicyclic pyrrolizidine backbone (Schramm et al., 2019), ruling out this alternative biosynthetic route (Figure 7). Our observations indicate that the second oxidation step is fast, as the pyrrolinium ion can only be detected as a minor intermediate in both *in vitro* assays and *in planta* incubations.

As a product of the HSO-catalyzed conversion of Hspd and as a further intermediate in PA biosynthesis, we have identified 1-formylpyrrolizidine (Figure 7). We provide evidence that the hydrogen peroxide resulting from the CuAO reaction mechanism is responsible for the nonenzymatic oxidation of 1-formylpyrrolizidine to 1-carboxypyrrolizidine. Such an oxidation of the aldehyde has also been described for other CuAOs with histamine as the substrate (Hough and Leurs, 2006). In the case of 1-formylpyrrolizidine, this nonenzymatic reaction seems to be relatively slow *in vitro*, as (1) 1-formylpyrrolizidine is the major product after the full oxidation of Hspd in the *in vitro* incubation with affinity-purified HSO and (2) even the addition of external hydrogen peroxide to 1-formylpyrrolizidine does not result in its complete conversion to 1-carboxypyrrolizidine. An open question is whether this nonenzymatic conversion is merely an *in vitro* artifact or occurs also *in planta*. In our tracer feeding experiments, we have found only trace amounts of 1-carboxypyrrolizidine, suggesting that 1-formylpyrrolizidine is converted so efficiently by successive enzymes of the pathway that hydrogen peroxide has only a minor effect. However, 1-carboxypyrrolizidine is incorporated, although with low efficiency, into trachelanthamide. The finding of methyl derivatives of 1-carboxypyrrolizidine, for example, chysin, in some other PA-producing plants (Lang et al., 2001; Woldemichael and Wink, 2002) suggests that the oxidation of 1-formylpyrrolizidine is also possible *in planta*.

### HSO controls stereospecific cyclization

In various alkaloid biosynthetic pathways, for example, tropane biosynthesis, the oxidation of amine precursors is followed by spontaneous cyclization (Hashimoto et al., 1990) (Figure 1). Moreover, spontaneous cyclization of the aminoaldehyde resulting from the oxidation of Hspd has been proposed for the formation of the pyrrolizidine backbone (Robins, 1982; Poupon et al., 2011; Lichman, 2021). This spontaneous cyclization might be involved in the formation of the monocyclic *N*-(4-aminobutyl)pyrrolinium ion. However, such spontaneous cyclization reactions occurring during the formation of the pyrrolizidine backbone with

two stereocenters (at C1 and C8) would result in a mixture of four diastereomers. Our data show that the HSO-catalyzed oxidation of Hspd results in the formation of only two stereoisomers of 1-formylpyrrolizidine, and that these are present in a ratio of about 10:1. This observation agrees with the finding that the PA structures described from a particular plant species are usually characterized by a necine base of only one defined stereochemical configuration (Cheng et al., 2011; Wesseling et al., 2017; Stegemann et al., 2018b). For instance, PAs extracted from *H. indicum* have retronecine, a derivative of (-)-trachelanthamide, as the necine base, whereas in grasses, PAs have been identified that have isoretronecanol as the base (Koulman et al., 2008). This stereochemical specificity supports an enzyme controlled mechanism, as postulated recently (Schramm et al., 2019; Lichman, 2021). As the two stereocenters at positions C1 and C8 along the pyrrolizidine backbone result from cyclization, we are tempted to conclude that the HSO controls the stereospecificity of the cyclization reaction without the involvement of any other enzyme. Future research should be directed to unraveling the molecular basis for the observed stereochemistry and to elucidating whether the described occurrence of PAs with a different stereochemistry in the necine base can be explained by a different stereospecificity of HSO. Furthermore, the impact of CuAOs on the biosynthesis of other natural compounds with complex cyclic structures has to be evaluated. For example, CuAOs have been postulated to be involved in the stereospecific formation of the bicyclic ring system of quinolizidine alkaloids (Golebiewski and Spenser, 1985; Wanner and Koomen, 1996).

### Possible compartmentalization of PA biosynthesis

In *H. indicum*, Hspd production by HSS is restricted to the lower leaf epidermis and to the epidermis of the shoots (Niemüller et al., 2012). In other tissues and in other non-PA-producing plants, Hspd is found only in traces and is regarded as a side-product of deoxyhypusine synthase, a paralog of HSS (Ober and Hartmann, 1999; Ober et al., 2003). However, although HSS has the capacity to produce substantial amounts of Hspd (Abdelhady et al., 2009), the accumulation of Hspd in the leaves of *H. indicum* is observed only after the inhibition of HSO (Frölich et al., 2007). Of note, the accumulated Hspd is exclusively incorporated into the PA indicine *N*-oxide after the inhibition of HSO is released (Frölich et al., 2007). This observation suggests that (1) HSO is not the rate-limiting step of PA biosynthesis, as it efficiently converts Hspd and (2) the accumulating Hspd does not act as a substrate for other enzymes of polyamine metabolism, suggesting strict compartmentalization, at least for this early step in PA biosynthesis. Further evidence for the compartmentalization of PA biosynthesis results from experiments with hairy roots of *Symphytum officinale* in which traces of Hspd, but not PAs, have been detected after the knockout of the HSS-coding gene (Zakaria et al., 2021). These low amounts of Hspd, most likely produced by deoxyhypusine synthase, are no substrate for PA biosynthesis in *S.*

*officinale*, thus supporting the concept of the compartmentalization of PA biosynthesis. The N-terminal signal peptide predicted to head HSO for vesicular transport indicates the localization of HSO in membrane-enclosed compartments. Further studies should clarify the role of the compartmentalization of HSO and of PA biosynthesis, especially with respect to the transport processes of polyamines that might be involved in the regulation of PA biosynthesis (Fujita and Shinozaki, 2014).

## Materials and methods

### Plant material and growth conditions

*Heliotropium indicum* was grown in a greenhouse under conditions as described previously (Kruse et al., 2017). Seeds of *N. benthamiana* were sown in pots containing TKS2 soil (Floragard, Germany) mixed with lava stones in a 3:1 ratio topped for germination with TKS1 soil. *Nicotiana benthamiana* plants were grown in a climate chamber (Johnson Control, Mannheim, Germany) equipped with ceramic metal halide lamps (CMT360LS WBH EYE Iwasaki Electric Co., Japan) at 25°C, 65% humidity, and a 16/8-h light/dark cycle (206  $\mu\text{mol m}^{-2} \text{s}^{-1}$ ). After 3 weeks, plants were fertilized (0.3%, v/v, Wuxal Top N fertilizer, Aglukon, Germany) and treated with Novo Nem F (ÖRE Bio-Protect, Schwentinental, Germany) for biological pest control until harvest.

### Relative transcript quantification

RNA extraction, cDNA synthesis, and RT-qPCR analysis of the genes of interest (GOI) encoding HSS, HSO, CuAO2, CuAO3, CuAO4, and CuAO5 were performed as described previously (Sievert et al., 2015) from *H. indicum* leaf epidermis sampled by laser capture microdissection microscopy. RT-qPCRs were performed in triplicate. The genes encoding actin, ubiquitin, and elongation factor 1 $\alpha$  were used as reference genes. Calculations of relative quantities, validation of reference genes, and normalization of the data followed (Remans et al., 2014). The geometric mean of the normalized relative quantities (NRQs) of the three reference genes was used as sample-specific factor to normalize the data of our GOIs. The average ( $n = 3$  RT-qPCR replicates) of NRQs of the GOIs relative to the upper epidermis (control group) was used to create the heat map in Figure 2A, illustrating expression differences between upper and lower epidermis. To test for effects in the VIGS experiments and to quantify the transcript level of the gene encoding the viral coat protein, RNA was extracted and used for cDNA synthesis and relative transcript quantification according to a method described by Kruse et al. (2019). As reference, the gene encoding ubiquitin was used, as it showed the most homogenous expression. The comparative  $C_T$  method was employed to calculate the transcript levels (Schmittgen and Livak, 2008). To determine the optimal time point for transient expression in *N. benthamiana* leaves, the gene encoding actin was used as a reference and the comparative  $C_T$  method was employed. Primer sequences are given in Supplemental Table S2.

### VIGS in *H. indicum*

VIGS experiments were conducted according to Dinesh-Kumar et al. (2003). Briefly, a sequence of  $\sim 300$  bp in length from the end of the open reading frame and the adjacent 3'-UTR was amplified using the primer pairs P33/P34 and P35/P36 for the cDNA encoding HSO and CuAO2, respectively (Supplemental Table S2), thereby introducing overhangs that allowed restriction cloning into the XhoI/NcoI-linearized pTRV2 vector. The resulting constructs, an empty vector control, and the pTRV1 vector were transformed independently into *A. tumefaciens* strain GV3101. Later developing leaves of *H. indicum* have a characteristic wrinkled surface structure (Supplemental Figure S1C). One to two of these leaves of 10-week-old plants (usually having approximately 7–8 well-developed leaves) were infected with a 1:1 mixture of two *A. tumefaciens* cultures that had been transformed with the pTRV2-based construct and the pTRV1, respectively. VIGS experiments were performed in two rounds. In Experiment 1 (performed in summer), the silencing effect of the HSO pTRV2 construct and an empty vector control (mock) was analyzed (three wild-type plants, three VIGS plants, and five mock plants) and in Experiment 2 (performed in early spring), the silencing effect of the CuAO2 pTRV2 construct was analyzed by comparing three wild-type plants with three VIGS plants. Three individual leaves that had not been used for the infection were harvested per plant and separately analyzed 1, 7, and 14 days after infection. Harvested leaves were ground in liquid nitrogen with a mortar and pestle to give a fine powder that was later used for RNA and alkaloid extraction. To test for systemic plant infection, the relative abundance of the TRV viral coat protein transcript was monitored according to Broderick and Jones (2014) with primer pair P18/P19 in RT-qPCRs. Mean  $\pm$  standard deviation ( $s_D$ ) of the log transformed  $\Delta C_T$  of the gene encoding the viral coat protein (*cp*) from triplicate PCRs were calculated (Supplemental Figure S12). TRV coat protein was detected after 7 days and was slightly elevated after 14 days. Therefore, to study a possible silencing effect, the transcript levels of *hso* and *hss* (experiment 1) and *cuao2* and *hss* (experiment 2) were determined in the leaves harvested 14 days after infection. For quantification of the *hso* and *cuao2* transcripts, primer pairs were used that did not bind to that part of the sequence used for the VIGS construct (P7/P9 and P10/P11, respectively). All primer sequences are given in Supplemental Table S2. First, means  $\pm$   $s_D$  of the log transformed  $\Delta C_T$  of *hss*, *hso*, and *cuao2* from triplicate RT-qPCRs were calculated.  $\Delta C_T$  of *hss* served as reference gene to monitor PA biosynthesis. Thus, in a second step, the  $\Delta C_T$  of *hso* and *cuao2* were normalized relative to  $\Delta C_T$  of *hss* ( $\Delta C_T_{hso}/\Delta C_T_{hss}$ ,  $\Delta C_T_{cuao2}/\Delta C_T_{hss}$ ). To calculate the  $s_D$  of these ratios, Gaussian error propagation was employed. Pearson's product correlation was used for correlation testing between *hss* and *hso* as well as *hss* and *cuao2* transcript levels. In parallel, PA concentration was analyzed in the leaves harvested 14 days after infection. Due to the limited plant material per leaf, PAs were quantified in a single assay by GC-MS as described previously

(Stegemann et al., 2018b). To test for differences between transcript levels and PA content in the groups “wild-type,” “mock,” and “VIGS” for the HSO construct (Experiment 1) and “wild-type” and “VIGS” for the CuAO2 construct (Experiment 2), normal distribution in the samples was tested by applying the Shapiro–Wilk test. The Welch 2 sample *t* test and the *t* test were used to compare samples with heterogeneity and homogeneity of variance, respectively. If normal distribution did not apply for a sample, comparisons were performed with the Mann–Whitney test. Statistical analyses were performed with XLSTAT (version 21.1.1, Addinsoft, New York, NY, USA) and RStudio (version 1.2.5019, RStudio Team, Boston, MA, USA). The detailed results of the statistical tests are provided in [Supplemental Data Set 1](#).

### Identification of complete open reading frames of HSO and CuAO2 and transient protein expression in *N. benthamiana*

Of the five transcripts of DAO-like sequences (CuAO1 to CuAO5) identified by a subtractive transcriptomics approach (Sievert et al., 2015), CuAO1 (=HSO) and CuAO2 were selected for transient expression in *N. benthamiana* plants. To obtain the full-length open reading frame, the 3'-end and the 5'-end of cDNA encoding HSO and CuAO2, respectively, were identified using the rapid amplification of cDNA ends approaches as described (Nurhayati et al., 2009). Primers are given in [Supplemental Table S2](#). For the prediction of N-terminal signal peptides, the SignalP-5.0 server (Almagro Armenteros et al., 2019b) and the TargetP-2.0 server (Almagro Armenteros et al., 2019a) were used. For the prediction of N-glycosylation sites the GlycoEP server (Chauhan et al., 2013) was used. The complete ORF of HSO (CuAO1) and CuAO2 were amplified using primer pairs P24/P25 and P26/P27, respectively, introducing attB1 and attB2 recombination sites, a Kozak sequence (Kanagarajan et al., 2012) directly in front of the start-ATG, and C-terminal Strep-tag II sequences (IBA, Göttingen, Germany). The resulting fragments were cloned into the binary vector pH7WG2D.1 (Karimi et al., 2007) using pDONR221 (Thermo Fisher Scientific, Waltham, MA, USA) as the entry vector. The resulting expression constructs were transformed into *A. tumefaciens* strain GV3101/pMP90 (Koncz and Schell, 1986) by electroporation, as were the empty pH7WG2D.1 vector as a control and the pBIN61-P19 vector that was used to minimize posttranslational silencing effects by co-infecting the *N. benthamiana* plants.

For transient protein expression in *N. benthamiana*, syringe agroinfiltration was performed using a method described by Broghammer et al. (2012) with modifications. Briefly, the infiltration medium (50 mM MES buffer, 2 mM Na<sub>3</sub>PO<sub>4</sub>, 0.5% glucose, 200 μM acetosyringone, pH 5.6) was employed to resuspend the pelleted agrobacterium harboring the vector plasmids before they were incubated for 2.5 h at room temperature. After diluting each culture to an optical density at 600 nm of 0.3, each of the cultures harboring

the expression vector was mixed with the culture harboring the pBIN61-P19 vector at a ratio of 3:1 for the infiltration of the leaves. The abaxial surface of the leaves was gently scratched with a syringe needle, and about 2-mL agrobacterium suspension was infiltrated into each leaf. For up to 50 plant individuals, several leaves per individual were infiltrated. Afterwards, plants were placed into a climate chamber (25°C, 65% humidity, and a 16/8-h light/dark cycle (206 μmol m<sup>-1</sup> s<sup>-1</sup>). Infiltrated leaves were harvested at 4 days (HSO) and 6 days (CuAO2) after infiltration and pooled for protein extraction. The optimal time point for harvest had been determined by quantifying transcript levels, protein levels, and enzymatic activity of the genes under study ([Supplemental Figure S2](#)).

### Protein extraction and purification

All steps were performed at 4°C if not stated otherwise. Leaf samples were frozen in liquid nitrogen and ground to a fine powder from which 1 g was extracted in 5 mL extraction buffer (100 mM Tris–HCl pH 8, 150 mM NaCl, 5% (w/v) polyvinylpyrrolidone, 2.5% (w/v) sodium ascorbate, 1% (w/v) activated charcoal, 2% (v/v) Bioblock to prevent binding of biotin to the affinity matrix) for 15 min at 4°C. After filtration of the extract via Miracloth (Merck-Millipore, Burlington, MA, USA), the extract was centrifuged at 20,000g for 20 min at 4°C. The extract was re-buffered by using centrifugal filter units of 30 kDa (Amicon, Merck, Darmstadt, Germany) to the assay buffer (30 mM potassium phosphate buffer, pH 7.2) or, for affinity purification, by using PD-10 desalting columns (GE Healthcare) to the purification buffer (100 mM Tris–HCl pH 8, 150 mM NaCl) before application onto a Strep-Tactin XT Superflow (IBA, Göttingen, Germany) with a flow rate of 7 drops/min. The protein concentration in the desalted crude protein extract was estimated using the method of Bradford (1976) or, in the case of purified protein, by direct absorption at 280 nm with the Nanodrop 2000 UV–Vis Spectrophotometer (Thermo Fisher Scientific).

### Protein gel blot analysis

Samples of 20 μg desalted crude protein extract were separated via sodium dodecylsulfate polyacrylamide gel electrophoresis (SDS–PAGE). The blotting step onto a polyvinylidene fluoride membrane (Immobilon P; Merck Millipore, Burlington, MA, USA) and the detection of the Strep-tag II by the Strep-Tactin AP conjugate (IBA, Göttingen, Germany, catalog # 2-1502-001) were performed as described by the manufacturer with the modification that the membrane was blocked overnight at room temperature with Tris-buffered saline supplemented with 0.1% (v/v) Tween-20, 0.1% (v/v) Triton, and 3% (w/v) bovine serum albumin and later incubated in Strep-Tactin AP Conjugate overnight at 4°C.

### Microsequencing of HSO

Affinity-purified HSO was separated by SDS–PAGE (0.5 μg per lane), cut from the gel after it had been stained with

Coomassie blue, and washed three times with water. Following digestion with trypsin, the resulting peptides were subjected to ESI-MS/MS as described previously (Roth et al., 2018).

### Photometrical assay for CuAO

An amount of 20  $\mu\text{g}$  purified enzyme in a total volume of 0.5 mL or 500  $\mu\text{g}$  desalted crude protein extract in a total volume of 0.75 mL was incubated for 5 and 15 min, respectively, in assay buffer (30 mM potassium phosphate buffer, pH 7.2) with 1 mM of each polyamine substrate (Hspd, Put, Spd, Spm, histamine, and Cad) at 30°C. Activity was quantified by the monitoring of hydrogen peroxide formation by color development (Allain et al., 1974). In the presence of horseradish peroxidase (5 U/mL, Carl Roth, Karlsruhe, Germany), the produced hydrogen peroxide oxidizes 4-aminoantipyrine, which couples to sodium 4-hydroxybenzenesulfonate dihydrate (25 mM, Sigma-Aldrich, St Louis, MO, USA) to form quinoneimine dye ( $\Delta\epsilon_{500} = 5.54 \text{ mM}^{-1} \text{ cm}^{-1}$ ) (Vojinović et al., 2004). Color formation was monitored continuously for 10 min by Swift-II software (GE Healthcare) to ensure linear product formation. Analyses with desalted crude protein extract were performed in comparison with extracts of leaves infected with empty vector as control.

### Site-directed mutagenesis

For site-directed mutagenesis, the construct containing the full ORF of HSO in the pDONR221 entry vector was amplified with the primer pair P31/P32 (Supplemental Table S2) by a method described previously (Liu and Naismith, 2008) to substitute the codon TAC by TTT, resulting in the replacement of tyrosine by phenylalanine. The modified sequence was introduced into the pH7WG2D.1 destination vector before being expressed as described for the unmodified sequences.

### Preparation of Hspd, [ $^{13}\text{C}$ ]Hspd, and [ $^{15}\text{N}$ ]Hspd

Hspd was prepared biosynthetically using the heterologously expressed bacterial HSS of *Blastochloris viridis* in *E. coli* (Tholl et al., 1996). In a total volume of 50 mL potassium phosphate buffer (50 mM, 2 mM DTT, 2 mM  $\text{NAD}^+$ , pH 8.6), 5 mg affinity-purified bacterial HSS was incubated with 5 mmol Put at 37°C overnight. Once the reaction had been stopped by the addition of 5.5 mL of 1.4 M hydrochloric acid, Hspd was purified using ion exchange resin as described previously (Ober et al., 2003), and the sample was tested for the complete removal of substrate by thin layer chromatography (Frölich et al., 2007). Following evaporation of the solvent, Hspd trihydrochloride powder was washed three times with methanol at 4°C to remove minor impurities. The identity and purity of Hspd were confirmed by 1D proton NMR, HMBC, and HSQC in  $\text{CDCl}_3$  (Carl Roth, Karlsruhe, Germany). The identical procedure was used to prepare [ $^{13}\text{C}$ ]Hspd and [ $^{15}\text{N}$ ]Hspd using fully labeled [ $^{13}\text{C}$ ]Put (Eurisotop, France) and fully labeled [ $^{15}\text{N}$ ]Put (Sigma-Aldrich), respectively, as substrates.

### Identification of the products of the HSO reaction

For the NMR-based identification of the product of the HSO-catalyzed conversion of Hspd, a protocol was chosen that had been described earlier for the identification of reaction products of BSAO (Houen et al., 2005). Briefly, 0.2 mg affinity-purified HSO (added in aliquots of 50  $\mu\text{g}$  every 12 h of incubation) was incubated in a total volume of 0.75 mL in potassium phosphate buffer (10 mM, pH 7.2) that was supplemented with 60  $\mu\text{L}$   $\text{D}_2\text{O}$  and that included 1 mM Hspd as a substrate, for 72 h at room temperature. In a second reaction, this protocol was modified with 40,000 U catalase (Carl Roth, Karlsruhe, Germany) being added to the reaction mix before the incubation was started and at each time point when HSO aliquots were also added (in total 160,000 U catalase) to catalyze the decomposition of hydrogen peroxide to water and oxygen. Enzymes were added repeatedly to the reaction mix to minimize the effects of protein denaturation and to increase product yield. The reaction was monitored via 1D proton NMR in 24-h time intervals.

For the GC-MS-based identification of the HSO reaction products, desalted crude protein extracts (5 mg) were incubated in a total volume of 1 mL in potassium phosphate buffer (30 mM, pH 7.2), which included 1 mM Hspd either with or without catalase (160,000 U/mL) at room temperature. The reaction was stopped at various time points by being flash-frozen in liquid nitrogen. For sample clean-up, the reactions were centrifuged (after being thawed) at  $14,000 \times g$  for 5 min at room temperature and applied to a Retain-SPE-CX cartridge (1 mg/3 mL, Thermo Fisher Scientific) according to the manufacturer's protocol. Of note, preacidification to pH 1–2 using 0.1 N sulfuric acid (Carl Roth, Karlsruhe, Germany) allowed the binding of all products of the various HSO-incubations, whereas the use of potassium phosphate buffer (30 mM, pH 7.2) allowed the binding of the 1-formylpyrrolizidine only. To exclude any impact on the conversion of Hspd by *N. benthamiana* proteins, the same set-up was repeated with an empty vector control.

To test the effect of hydrogen peroxide on the product composition of the HSO reaction, purified 1-formylpyrrolizidine was resuspended in potassium phosphate buffer (30 mM, pH 7.2) containing 2 mM hydrogen peroxide (Carl Roth, Karlsruhe, Germany) and incubated for 1 h at room temperature. After preacidification to pH 1–2 using 0.1 N sulfuric acid (Carl Roth, Karlsruhe, Germany), 1-formylpyrrolizidine and 1-carboxypyrrolizidine were purified via a Retain-SPE-CX cartridge (1 mg/3 mL, Thermo Fisher Scientific). For unequivocal product identification, the products resulting from the incubation of Hspd with purified HSO were derivatized with MOX and MSTFA to confirm the presence of the aldehyde group and the carboxy group in 1-formylpyrrolizidine and 1-carboxypyrrolizidine, respectively. Thus, the purified reaction products were reconstituted in methanol, dried under an air stream, and then reconstituted in 30  $\mu\text{L}$  MOX reagent (Thermo Fisher Scientific) and incubated for 1 h at 37°C. After the addition

of 15  $\mu$ L MSTFA (Thermo Fisher Scientific), the sample was incubated for another 30 min at 37°C.

### NMR Analyses

1D and 2D proton NMR spectra for observation of the reaction process were recorded using a Bruker Avance III 300 NMR spectrometer (Bruker, Rheinstetten, Germany) operating at 300 MHz for  $^1\text{H}$ , 75.5 MHz for  $^{13}\text{C}$ , and 30.4 MHz for  $^{15}\text{N}$ , a Bruker Avance III 400 NMR spectrometer operating at 400 MHz for  $^1\text{H}$  and 101 MHz for  $^{13}\text{C}$ , a Bruker Avance III 500 NMR spectrometer operating at 500 MHz for  $^1\text{H}$ , 126 MHz for  $^{13}\text{C}$ , and 50.7 MHz for  $^{15}\text{N}$ , or a Bruker Avance 600 spectrometer with CryoProbe operating at 600 MHz for  $^1\text{H}$ , 151 MHz for  $^{13}\text{C}$ , and 60.8 MHz for  $^{15}\text{N}$ . Measurements were performed at 298 K, and the temperature was calibrated with a methanol- $d_4$  solution. For each sample, automatic tuning and matching of the probe were performed, in addition to automatic shimming. Standard pulse programs of the manufacturer's pulse program library were used.

### Tracer-feeding experiments

For tracer feeding a method described earlier was used (Stegemann et al., 2018a) with [ $^{13}\text{C}$ ]Hspd and the two products of the HSO reaction, that is, [ $^{13}\text{C}$ ]1-formylpyrrolizidine and [ $^{13}\text{C}$ ]1-carboxypyrrolizidine, as tracers. To enhance [ $^{13}\text{C}$ ]1-formylpyrrolizidine formation, catalase was added, and the product was purified by means of potassium phosphate buffer (30 mM, pH 7.2) to allow the binding of the 1-formylpyrrolizidine only as described above. To obtain [ $^{13}\text{C}$ ]1-carboxypyrrolizidine, an HSO incubation without catalase using desalted crude protein extract for 20 h (see above) was used for another incubation with 2 mM hydrogen peroxide for 60 min in order completely to oxidize the [ $^{13}\text{C}$ ]1-formylpyrrolizidine before purification as described above. Pathway intermediates and PA patterns were identified by GC–MS as described earlier (Stegemann et al., 2018b).

### GC–EI–HRAMS

The exact molecular weight and molecular formula of the HSO reaction products were determined using a QExactive GC–Orbitrap instrument (Thermo Fisher Scientific, Dreieich) with the electron-impact ion source temperature at 280°C. Scans (100–200  $m/z$ ) were performed at a resolution of 60,000 (at 200  $m/z$ ) and 70 eV. GC parameters were as follows: SSL injector temperature: 280°C, carrier gas helium with a flow of 1.2 mL/min; split flow: 25 mL/min, transferline temperature: 280°C; oven program: 45°C hold 1 min, 35°C/min to 300°C, 300°C hold 2 min; GC column: TG-5 SilMS 30 m, 0.25 mm, 0.25  $\mu$ m.

### Accession numbers

Sequence data from this article have been deposited with the GenBank data library under the following accession numbers: *Heliotropium indicum* HSO (MT597432), CuAO2 (MT627598), CuAO3 (MT627599), CuAO4 (MT627600), and CuAO5 (MT627601).

## Supplemental data

The following materials are available in the online version of this article.

**Supplemental Figure S1.** Relative expression profile of CuAOs in leaves of *H. indicum* wild-type plants and plants subjected to VIGS.

**Supplemental Figure S2.** Estimation of expression levels after transient infection of *N. benthamiana* leaves in days post infection.

**Supplemental Figure S3.** Kinetic properties of HSO.

**Supplemental Figure S4.** Detection of the posttranslationally synthesized cofactor TPQ of HSO.

**Supplemental Figure S5.** Detection of *N*-glycosylation of HSO exemplified for the second glycosylation site.

**Supplemental Figure S6.** 2D NMR with HSQC and H,H-COSY spectra of the reaction products of HSO with Hspd as substrate.

**Supplemental Figure S7.** HSQC spectrum of the purified reaction product resulting from incubation of HSO with Hspd after repetitive addition of catalase.

**Supplemental Figure S8.** 126 MHz  $^1\text{H}$  decoupled  $^{13}\text{C}$ -NMR spectra of an incubation of HSO with Hspd without and with addition of catalase.

**Supplemental Figure S9.** Characterization of [ $^{15}\text{N}$ ]Hspd.

**Supplemental Figure S10.** Characterization of the amino groups of the substrate Hspd and the HSO reaction products.

**Supplemental Figure S11.** Derivatization of HSO-reaction product mixture with MOX and MSTFA.

**Supplemental Figure S12.** Relative TRV coat protein transcript abundance ( $\Delta\text{C}_T$ ) in leaves of *H. indicum* infected with *A. tumefaciens* carrying VIGS constructs.

**Supplemental Table S1.** Kinetic data of HSO and CuAO2 analyzed using different models in GraphPad Prism (version 8.4.3 (686), San Diego, CA, USA).

**Supplemental Table S2.** Primer sequences.

**Supplemental Data Set 1.** Test statistics for VIGS Experiments 1 and 2.

## Acknowledgments

We are grateful to Dr Frank Sönnichsen for help with the interpretation of NMR data, and Dr Axel Scheidig for discussions concerning the biochemistry of CuAOs. We thank Brigitte Schemmerling, Hilke Duin, Stephanie Käther, and Daniel Bross for their assistance in the lab.

## Funding

This work was supported by a German Egyptian Research Long-term fellowship to M.M.Z. and by a grant of the German Research Foundation to D.O. (Deutsche Forschungsgemeinschaft, DFG, OB 162/7-2).

*Conflict of interest statement.* None declared.



## References

- Abdelhady MIS, Beuerle T, Ober D (2009) Homospermidine in transgenic tobacco results in considerably reduced spermidine levels but is not converted to pyrrolizidine alkaloid precursors. *Plant Mol Biol* **71**: 145–155
- Allain CC, Poon LS, Chan CS, Richmond W, Fu PC (1974) Enzymatic determination of total serum cholesterol. *Clin Chem* **20**: 470–475
- Almagro Armenteros JJ, Salvatore M, Emanuelsson O, Winther O, von Heijne G, Elofsson A, Nielsen H (2019a) Detecting sequence signals in targeting peptides using deep learning. *Life Sci Alliance* **2**: e201900429
- Almagro Armenteros JJ, Tsigirgos KD, Sonderby CK, Petersen TN, Winther O, Brunak S, von Heijne G, Nielsen H (2019b) SignalP 5.0 improves signal peptide predictions using deep neural networks. *Nat Biotechnol* **37**: 420–423
- Aniszewski T (2007) Alkaloid chemistry. *Alkaloids - Secrets of Life*, Elsevier, Amsterdam, the Netherlands, pp 61–139
- Anke S, Niemüller D, Moll S, Hänsch R, Ober D (2004) Polyphyletic origin of pyrrolizidine alkaloids within the Asteraceae. Evidence from differential tissue expression of homospermidine synthase. *Plant Physiol* **136**: 4037–4047
- Anke S, Gonde D, Kaltenecker E, Hansch R, Theuring C, Ober D (2008) Pyrrolizidine alkaloid biosynthesis in *Phalaenopsis* orchids: developmental expression of alkaloid-specific homospermidine synthase in root tips and young flower buds. *Plant Physiol* **148**: 751–760
- Bardsley WG, Crabbe MJ, Shindler JS (1973) Kinetics of the diamine oxidase reaction. *Biochem J* **131**: 459–469
- Böttcher F, Adolph RD, Hartmann T (1993) Homospermidine synthase, the first pathway-specific enzyme in pyrrolizidine alkaloid biosynthesis. *Phytochemistry* **32**: 679–689
- Bradford MM (1976) A rapid and sensitive method for the quantitation of microgram quantities of protein utilizing the principle of protein-dye binding. *Anal Biochem* **72**: 248–254
- Broderick SR, Jones ML (2014) An optimized protocol to increase virus-induced gene silencing efficiency and minimize viral symptoms in *Petunia*. *Plant Mol Biol Rep* **32**: 219–233
- Broghammer A, Krusell L, Blaise M, Sauer J, Sullivan JT, Maolanon N, Vinther M, Lorentzen A, Madsen EB, Jensen KJ, et al. (2012) Legume receptors perceive the rhizobial lipochitin oligosaccharide signal molecules by direct binding. *Proc Natl Acad Sci USA* **109**: 13859–13864
- Chauhan JS, Rao A, Raghava GP (2013) *In silico* platform for prediction of N-, O- and C-glycosites in eukaryotic protein sequences. *PLoS One* **8**: e67008
- Chen D, Shao Q, Yin L, Younis A, Zheng B (2018) Polyamine function in plants: metabolism, regulation on development, and roles in abiotic stress responses. *Front Plant Sci* **9**: 1945
- Cheng D, Kirk H, Vrieling K, Mulder PPJ, Klinkhamer PGL (2011) The relationship between structurally different pyrrolizidine alkaloids and western flower thrips resistance in F(2) hybrids of *Jacobaea vulgaris* and *Jacobaea aquatica*. *J Chem Ecol* **37**: 1071–1080
- Cogoni A, Padiglia A, Medda R, Segni P, Floris G (1991) Oxidation of spermine by an amine oxidase from lentil seedlings. *Plant Physiol* **95**: 477–479
- Dinesh-Kumar SP, Anandalakshmi R, Marathe R, Schiff M, Liu Y (2003) Virus-induced gene silencing. *Methods Mol Biol* **236**: 287–294
- Franc V, Řehulka P, Medda R, Padiglia A, Floris G, Šebela M (2013) Analysis of the glycosylation pattern of plant copper amine oxidases by MALDI-TOF/TOF MS coupled to a manual chromatographic separation of glycans and glycopeptides. *Electrophoresis* **34**: 2357–2367
- Fraudentali I, Ghuge SA, Carucci A, Tavladoraki P, Angelini R, Cona A, Rodrigues-Pousada RA (2019) The copper amine oxidase AtCuAO-participates in abscisic acid-induced stomatal closure in *Arabidopsis*. *Plants* **8**: 183
- Frölich C, Ober D, Hartmann T (2007) Tissue distribution, core biosynthesis and diversification of pyrrolizidine alkaloids of the lycopsamine type in three Boraginaceae species. *Phytochemistry* **68**: 1026–1037
- Fujita M, Shinozaki K (2014) Identification of polyamine transporters in plants: paraquat transport provides crucial clues. *Plant Cell Physiol* **55**: 855–861
- Gerdes HJ, Leistner E (1979) Stereochemistry of reactions catalysed by L-lysine decarboxylase and diamine oxidase. *Phytochemistry* **18**: 771–775
- Ghughe SA, Tisi A, Carucci A, Rodrigues-Pousada RA, Franchi S, Tavladoraki P, Angelini R, Cona A (2015) Cell wall amine oxidases: new players in root xylem differentiation under stress conditions. *Plants* **4**: 489–504
- Golebiewski WM, Spenser ID (1985) Biosynthesis of the lupine alkaloids. I. Lupinine. *Can J Chem* **63**: 2707–2718
- Gross F, Rudolf EE, Thiele B, Durner J, Astier J (2017) Copper amine oxidase 8 regulates arginine-dependent nitric oxide production in *Arabidopsis thaliana*. *J Exp Bot* **68**: 2149–2162
- Hashimoto T, Mitani A, Yamada Y (1990) Diamine oxidase from cultured roots of *Hyoscyamus niger*: its function in tropane alkaloid biosynthesis. *Plant Physiol* **93**: 216–221
- Heim WG, Sykes KA, Hildreth SB, Sun J, Lu RH, Jelesko JG (2007) Cloning and characterization of a *Nicotiana tabacum* methylputrescine oxidase transcript. *Phytochemistry* **68**: 454–463
- Houen G, Struve C, Sondergaard R, Friis T, Anthoni U, Nielsen PH, Christophersen C, Petersen BO, Duus JO (2005) Substrate specificity of the bovine serum amine oxidase and in situ characterisation of aminoaldehydes by NMR spectroscopy. *Bioorg Med Chem* **13**: 3783–3796
- Hough L, Leurs R (2006) Histamine. In GJ Siegel, RW Albers, ST Brady, and DL Price, eds, *Basic Neurochemistry. Molecular, Cellular and Medical Aspects*, Elsevier, Amsterdam, the Netherlands, pp 249–266
- Ignesti G (2003) Equations of substrate-inhibition kinetics applied to pig kidney diamine oxidase (DAO, E.C. 1.4.3.6). *J Enzyme Inhibit Med Chem* **18**: 463–473
- Johnson BJ, Cohen J, Welford RW, Pearson AR, Schulten K, Klinman JP, Wilmot CM (2007) Exploring molecular oxygen pathways in *Hansenula polymorpha* copper-containing amine oxidase. *J Biol Chem* **282**: 17767–17776
- Kaltenecker E, Eich E, Ober D (2013) Evolution of homospermidine synthase in the Convolvulaceae: a story of gene duplication, gene loss, and periods of various selection pressures. *Plant Cell* **25**: 1213–1227
- Kanagarajan S, Tolf C, Lundgren A, Waldenstrom J, Brodelius PE (2012) Transient expression of hemagglutinin antigen from low pathogenic avian influenza A (H7N7) in *Nicotiana benthamiana*. *PLoS One* **7**: e33010
- Karimi M, Depicker A, Hilson P (2007) Recombinational cloning with plant gateway vectors. *Plant Physiol* **145**: 1144–1154
- Katoh A, Shoji T, Hashimoto T (2007) Molecular cloning of N-methylputrescine oxidase from tobacco. *Plant Cell Physiol* **48**: 550–554
- Kelly HA, Robins DJ (1988) Evidence for an immonium ion intermediate in pyrrolizidine alkaloid biosynthesis. *Chem Commun* **1988**: 329–330
- Khan HA, Robins DJ (1985) Pyrrolizidine alkaloid biosynthesis. Synthesis of <sup>14</sup>C-labelled homospermidines and their incorporation into retronecine. *J Chem Soc Perkin Trans* **1**: 819–824
- Koncz C, Schell J (1986) The promoter of TL-DNA gene 5 controls the tissue-specific expression of chimaeric genes carried by a novel type of *Agrobacterium* binary vector. *Mol Gen Genet* **204**: 383–396
- Koulman A, Seeliger C, Edwards PJB, Fraser K, Simpson W, Johnson L, Cao M, Rasmussen S, Lane GA (2008)

- E/Z-Thesinine-O-4'-a-ribose, pyrrolizidine conjugates produced by grasses (Poaceae). *Phytochemistry* **69**: 1927–1932
- Koyanagi T, Matsumura K, Kuroda SI, Tanizawa K** (2000) Molecular cloning and heterologous expression of pea seedling copper amine oxidase. *Biosci Biotech Biochem* **64**: 717–722
- Kruse LH, Stegemann T, Sievert C, Ober D** (2017) Identification of a second site of pyrrolizidine alkaloid biosynthesis in Comfrey to boost plant defense in floral stage. *Plant Physiol* **174**: 47–55
- Kruse LH, Stegemann T, Jensen-Kroll J, Engelhardt A, Wesseling AM, Lippert A, Ludwig-Müller J, Ober D** (2019) Reduction of pyrrolizidine alkaloid levels in comfrey (*Symphytum officinale*) hairy roots by RNAi silencing of homospermidine synthase. *Planta Med* **85**: 1177–1186
- Kumar V, Dooley DM, Freeman HC, Guss JM, Harvey I, McGuirl MA, Wilce MC, Zubak VM** (1996) Crystal structure of a eukaryotic (pea seedling) copper-containing amine oxidase at 2.2 Å resolution. *Structure* **4**: 943–955
- Lang G, Passreiter CM, Medinilla B, Castillo JJ, Witte L** (2001) Non-toxic pyrrolizidine alkaloids from *Eupatorium semialatum*. *Biochem Syst Ecol* **29**: 143–147
- Li R, Klinman JP, Mathews FS** (1998) Copper amine oxidase from *Hansenula polymorpha*: the crystal structure determined at 2.4 Å resolution reveals the active conformation. *Structure* **6**: 293–307
- Lichman BR** (2021) The scaffold-forming steps of plant alkaloid biosynthesis. *Nat Prod Rep* **38**: 103–129
- Liu H, Naismith JH** (2008) An efficient one-step site-directed deletion, insertion, single and multiple-site plasmid mutagenesis protocol. *BMC Biotechnol* **8**: 91
- Lunelli M, Di Paolo ML, Biadene M, Calderone V, Battistutta R, Scarpa M, Rigo A, Zanotti G** (2005) Crystal structure of amine oxidase from bovine serum. *J Mol Biol* **346**: 991–1004
- Ma X, Gang DR** (2004) The Lycopodium alkaloids. *Nat Prod Rep* **21**: 752–772
- Medda R, Bellelli A, Pec P, Federico R, Cona A, Floris G** (2009) In Copper Amine Oxidases, G Floris and B Mondovì, eds, Copper Amine Oxidases from Plants, CRC Press, Boca Raton, FL, pp 39–50
- Michael AJ** (2016) Polyamines in eukaryotes, bacteria, and archaea. *J Biol Chem* **291**: 14896–14903
- Moll S, Anke S, Kahmann U, Hänsch R, Hartmann T, Ober D** (2002) Cell-specific expression of homospermidine synthase, the entry enzyme of the pyrrolizidine alkaloid pathway in *Senecio vernalis*, in comparison with its ancestor, deoxyhypusine synthase. *Plant Physiol* **130**: 47–57
- Moschou PN, Wu J, Cona A, Tavladoraki P, Angelini R, Roubelakis-Angelakis KA** (2012) The polyamines and their catabolic products are significant players in the turnover of nitrogenous molecules in plants. *J Exp Bot* **63**: 5003–5015
- Nagakubo T, Kumano T, Ohta T, Hashimoto Y, Kobayashi M** (2019) Copper amine oxidases catalyze the oxidative deamination and hydrolysis of cyclic imines. *Nat Commun* **10**: 413
- Niemüller D, Reimann A, Ober D** (2012) Distinct cell-specific expression of homospermidine synthase involved in pyrrolizidine alkaloid biosynthesis in three species of the Boraginales. *Plant Physiol* **159**: 920–929
- Nurhayati N, Gondé D, Ober D** (2009) Evolution of pyrrolizidine alkaloids in *Phalaenopsis* orchids and other monocotyledons: identification of deoxyhypusine synthase, homospermidine synthase and related pseudogenes. *Phytochemistry* **70**: 508–516
- Ober D, Hartmann T** (1999) Homospermidine synthase, the first pathway-specific enzyme of pyrrolizidine alkaloid biosynthesis, evolved from deoxyhypusine synthase. *Proc Natl Acad Sci USA* **96**: 14777–14782
- Ober D, Hartmann T** (2000) Phylogenetic origin of a secondary pathway: the case of pyrrolizidine alkaloids. *Plant Mol Biol* **44**: 445–450
- Ober D, Gibas L, Witte L, Hartmann T** (2003) Evidence for general occurrence of homospermidine in plants and its supposed origin as by-product of deoxyhypusine synthase. *Phytochemistry* **62**: 339–344
- Pietrangeli P, Federico R, Mondovì B, Morpurgo L** (2007) Substrate specificity of copper-containing plant amine oxidases. *J Inorg Biochem* **101**: 997–1004
- Poupon E, Salame R, Yan LH** (2011) Biomimetic synthesis of ornithine/arginine and lysine-derived alkaloids: selected examples. In E Poupon and B Nay, eds, Biomimetic Organic Synthesis, Wiley, Hoboken, NJ, pp 1–60
- Reimann A, Nurhayati N, Backenköhler A, Ober D** (2004) Repeated evolution of the pyrrolizidine alkaloid-mediated defense system in separate angiosperm lineages. *Plant Cell* **16**: 2772–2784
- Remans T, Keunen E, Bex GJ, Smeets K, Vangronsveld J, Cuypers A** (2014) Reliable gene expression analysis by reverse transcription-quantitative PCR: reporting and minimizing the uncertainty in data accuracy. *Plant Cell* **26**: 3829–3837
- Rinaldi AC, Porcu CM, Oliva S, Curreli N, Rescigno A, Sollai F, Rinaldi A, Finazzi-Agró A, Sanjust E** (1998) Biosynthesis of the topaquinone cofactor in copper amine oxidases. *Eur J Biochem* **251**: 91–97
- Robins DJ** (1982) A biogenetically patterned synthesis of the pyrrolizidine alkaloid trachelanthamidine. *J Chem Soc Chem Commun* **1982**: 1289–1290
- Roth G, Vanz AL, Lünsdorf H, Nimtz M, Rinas U** (2018) Fate of the UPR marker protein Kar2/Bip and autophagic processes in fed-batch cultures of secretory insulin precursor producing *Pichia pastoris*. *Microbial Cell Fact* **17**: 123
- Schmittgen TD, Livak KJ** (2008) Analyzing real-time PCR data by the comparative C(T) method. *Nat Protoc* **3**: 1101–1108
- Schramm S, Kohler N, Rozhon W** (2019) Pyrrolizidine alkaloids: biosynthesis, biological activities and occurrence in crop plants. *Molecules* **24**: 498
- Sebela M, Sayre LM** (2009) Inhibitors of copper amine oxidases: past, present, and future. In G Floris and B Mondovì, eds, Copper Amine Oxidases, CRC Press, Boca Raton, FL, pp 219–237
- Seiler N, Raul F** (2005) Polyamines and apoptosis. *J Cell Mol Med* **9**: 623–642
- Sievert C, Beuerle T, Hollmann J, Ober D** (2015) Single cell subtractive transcriptomics for identification of cell-specifically expressed candidate genes of pyrrolizidine alkaloid biosynthesis. *Phytochemistry* **117**: 17–24
- Sobieszczuk-Nowicka E, Paluch-Lubawa E, Mattoo AK, Arasimowicz-Jelonek M, Gregersen PL, Pacak A** (2019) Polyamines - a new metabolic switch: crosstalk with networks involving senescence, crop improvement, and mammalian cancer therapy. *Front Plant Sci* **10**: 859
- Stegemann T, Kruse LH, Ober D** (2018a) Radioactive tracer feeding experiments and product analysis to determine the biosynthetic capability of Comfrey (*Symphytum officinale*) leaves for pyrrolizidine alkaloids. *Bio-protocol* **8**: e2719
- Stegemann T, Kruse LH, Brütt M, Ober D** (2018b) Specific distribution of pyrrolizidine alkaloids in floral parts of comfrey (*Symphytum officinale*) and its implications for flower ecology. *J Chem Ecol* **45**: 128–135
- Strasser R** (2016) Plant protein glycosylation. *Glycobiology* **26**: 926–939
- Tavladoraki P, Cona A, Angelini R** (2016) Copper-containing amine oxidases and FAD-dependent polyamine oxidases are key players in plant tissue differentiation and organ development. *Front Plant Sci* **7**: 824
- Tholl D, Ober D, Martin W, Kellermann J, Hartmann T** (1996) Purification, molecular cloning and expression in *Escherichia coli* of homospermidine synthase from *Rhodospseudomonas viridis*. *Eur J Biochem* **240**: 373–379

- Tipping AJ, McPherson MJ** (1995) Cloning and molecular analysis of the pea seedling copper amine oxidase. *J Biol Chem* **270**: 16939–16946
- Vojinović V, Azevedo AM, Martins VCB, Cabral JMS, Gibson TD, Fonseca LP** (2004) Assay of H<sub>2</sub>O<sub>2</sub> by HRP catalysed co-oxidation of phenol-4-sulphonic acid and 4-aminoantipyrine: characterisation and optimisation. *J Mol Catal B Enzym* **28**: 129–135
- Wanner MJ, Koomen GJ** (1996) Oxidative deamination of tetrahydroanabasine with o-quinones: an easy entry to lupinine, sparteine, and anabasine. *J Org Chem* **61**: 5581–5586
- Wanner MJ, Koomen GJ** (1999) Evolution-based synthesis of racemic alkaloids. *Pure Appl Chem* **70**: 2129
- Wesseling AM, Demetrowitsch TJ, Schwarz K, Ober D** (2017) Variability of pyrrolizidine alkaloid occurrence in species of the grass subfamily Pooideae (Poaceae). *Front Plant Sci* **8**: 2046
- Woldemichael GM, Wink M** (2002) Concomitant occurrence of pyrrolizidine and quinolizidine alkaloids in the hemiparasite *Osyris alba* L. (Santalaceae). *Biochem Syst Ecol* **30**: 139–149
- Yang T, Nagy I, Mancinotti D, Otterbach SL, Andersen TB, Motawia MS, Asp T, Geu-Flores F** (2017) Transcript profiling of a bitter variety of narrow-leaved lupin to discover alkaloid biosynthetic genes. *J Exp Bot* **68**: 5527–5537
- Zakaria MM, Schemmerling B, Ober D** (2021) CRISPR/Cas9-mediated genome editing in comfrey (*Symphytum officinale*) hairy roots results in the complete eradication of pyrrolizidine alkaloids. *Molecules* **26**: 1498
- Zarei A, Trobacher CP, Cooke AR, Meyers AJ, Hall JC, Shelp BJ** (2015) Apple fruit copper amine oxidase isoforms: peroxisomal MdAO1 prefers diamines as substrates, whereas extracellular MdAO2 exclusively utilizes monoamines. *Plant Cell Physiol* **56**: 137–147